PERGAMON

International Journal of Solids and Structures 38 (2001) 6559–6588

INTERNATIONAL JOURNAL OF SOLIDS and STRUCTURES

www.elsevier.com/locate/ijsolstr

The problem for bonded half-planes containing a crack at an arbitrary angle to the graded interfacial zone

Hyung Jip Choi *

School of Mechanical and Automotive Engineering, Kookmin University, 861-1 Chongnung-Dong, Songbuk-Gu, Seoul 136-702, South Korea

Received 7 April 2000; in revised form 13 April 2001

Abstract

The plane problem for bonded elastic half-planes containing a crack at an arbitrary angle to the graded interfacial zone is considered in this paper. The interfacial zone is treated as a nonhomogeneous interlayer with its elastic modulus varying continuously in thickness direction. Based on the use of the Fourier integral transform method and with the aid of the stiffness matrix approach, the crack problem is formulated as a system of singular integral equations for arbitrary crack surface tractions. The main results presented are the variations of mixed-mode stress intensity factors as a function of the crack orientation angle for various combinations of material and geometric parameters of bonded media in conjunction with the nonhomogeneity in the graded interlayer. The probable cleavage angles for the crack growth direction are also evaluated under the remote biaxial loading, together with the corresponding values of effective tensile mode stress intensity factors.

Keywords: Bonded media; Inclined crack; Functionally graded materials; Interfacial zone; Singular integral equations; Stress intensity factors

1. Introduction

The analysis of functionally graded materials has become a subject of increasing importance motivated by a number of potential benefits achievable from the use of such novel materials in a wide range of modern technological practices. The major advantages of the graded material, especially in elevated temperature environments, stem from the tailoring capability to produce a gradual variation of its thermomechanical properties in the spatial domain (Koizumi, 1993). In particular, the use of the graded material as interlayers in the bonded media is one of the highly effective and promising applications in eliminating various shortcomings resulting from stepwise property mismatch inherent in piecewise homogeneous composite media (Lee and Erdogan, 1994; Suresh and Mortensen, 1997).

* Tel.: +82-2-910-4682; fax: +82-2-910-4839.
E-mail address: hjchoi@kmu.kookmin.ac.kr (H.J. Choi).

0020-7683/01/$ - see front matter
PII: S0020-7683(01)00090-7

From the fracture mechanics viewpoint, the presence of a graded interlayer would play an important role in determining the crack driving forces and fracture resistance parameters. In an attempt to address the issues pertaining to the fracture analysis of bonded media with such transitional interfacial properties, a series of solutions to certain crack problems was obtained by Erdogan and his associates. Among them are a crack in the nonhomogeneous interlayer bounded by dissimilar homogeneous media (Delale and Erdogan, 1988); a crack perpendicular to and approaching the interface with a nonhomogeneous medium (Erdogan et al., 1991); and a crack at the interface between homogeneous and nonhomogeneous materials (Chen, 1990; Ozturk and Erdogan, 1996). Similar problems of delamination or an interface crack between the functionally graded coating and the substrate were considered by Jin and Batra (1996), Bao and Cai (1997), and Shbeeb and Binienda (1999). Besides, the analysis of a crack normal to the graded interfacial zone in the layered half-plane and bonded strips was performed by Choi (1996a,b). More recently, the interaction of collinear cracks in a layered medium with a graded interlayer subjected to mechanical and thermal shock loading was reported by Choi et al. (1998a,b), and the dynamic responses of a crack in functionally graded materials are due to Babaei and Lukasiewicz (1998) and Parameswaran and Shukla (1999). Gu and Asaro (1997), based on the local homogeneity of such materials in the near-tip field, examined the crack deflection for several cracked geometries.

A significant implication from all these studies is that the near-tip singular stress field remains to be of the square-root type along with the same angular distributions around the crack tip as those for homogeneous materials, independent of the crack orientation when the spatial distribution of the elastic properties is continuous and piecewise differentiable near and at the crack tip. As a result, the influence of material gradients in the vicinity of a crack tip manifests itself through the stress intensity factors. For more details, interested readers are referred to the work by Atkinson (1977), Eischen (1987), Schovanec and Walton (1988), Erdogan et al. (1991), Martin (1992), and Jin and Noda (1994). It should be reminded that this rectifies such pathological drawback as oscillatory or nonsquare-root stress singularities that occur in analyzing the bonded materials which are assumed to be piecewise homogeneous with an ideal interface of zero thickness (Rice, 1988; Romeo and Ballarini, 1995).

As aforementioned, the preceding analyses of crack problems for bonded media with the graded properties are ordinarily restricted to two particular crack orientations, for which the geometric, material, and loading symmetries exist about the crack plane or about the normal through the crack center. It appears that the near-tip field quantities for an arbitrarily oriented crack entailing the presence of the graded interlayer are not yet available; although a number of previous analytical solutions for the inclined crack in the single phase media are well documented in the literature, for example, by Krenk (1975), Erdogan and Arin (1975), Delale et al. (1979), Kim and Lee (1996), Rayaprolu and Rooke (1998), and Beghini et al. (1999), while those in the piecewise homogeneous bonded media have been obtained using different techniques, e.g., by Bogy (1971), Erdogan and Aksogan (1974), Ashbaugh (1975), Isida and Noguchi (1993), Wang and Meguid (1996), and the references therein.

The objective of this paper is, therefore, to provide a plane elasticity solution for an inclined crack in the bonded dissimilar half-planes with a graded nonhomogeneous interfacial zone. The Fourier integral transform method is employed and the formulation of the crack problem with the aid of the stiffness matrix approach results in a system of singular integral equations for arbitrary crack surface tractions. The mixed-mode stress intensity factors are defined in terms of the solutions to the integral equations. In the numerical results, parametric studies are conducted so that the stress intensity factors are evaluated as a function of the crack orientation angle for various material and geometric combinations of the bonded media. Both the uniform crack surface tractions and the remote biaxial loading are considered as the external boundary conditions. Further presented are the probable cleavage angles for the crack growth direction under the biaxial loading condition and the corresponding values of effective tensile-mode stress intensity factors.

2. Problem statement and formulation

Consider the elastic half-planes bonded through an interfacial zone with the graded properties. As shown in Fig. 1, a half-plane in the right-hand side contains a crack at an arbitrary angle θ to the graded interfacial zone. The two rectangular Cartesian coordinate systems, (x, y) and (x_1, y_1), are employed which are related to each other as

$$x_1 = mx + ny, \quad y_1 = -nx + my \tag{1a}$$

$$m = \cos\theta, \quad n = \sin\theta \tag{1b}$$

where the angle θ is measured counterclockwise from the positive x-axis. In the (x_1, y_1) coordinate, the crack is located along the line at $a < x_1 < b$ and $y_1 = 0$, with its length and distance from the interfacial zone being $2c = b - a$ and d, respectively. Thus, for a fixed distance d, the crack can be oriented from a perpendicular position ($\theta = 0°$) to a parallel or an interfacial one ($\theta = 90°$) in the bonded media. The cracked half-plane, the interfacial zone, and the uncracked half-plane are distinguished in order from the right-hand side and are defined in the (x, y) coordinate system.

By denoting the elastic moduli of the dissimilar homogeneous half-planes as E_j, $j = 1, 3$, and modeling the graded interfacial zone as a nonhomogeneous interlayer of thickness h, the elastic modulus of the interlayer $E_2(x)$ is approximated based largely on analytical expediency as (Ozturk and Erdogan, 1996)

$$E_2(x) = E_o\, e^{\beta x} \tag{2}$$

where the constant E_o and the nonhomogeneity parameter β are specified satisfying the continuous transition of the elastic moduli from one half-plane to the other as

$$E_o = E_1, \quad \beta = -\frac{1}{h} \ln\left(\frac{E_3}{E_1}\right) \tag{3}$$

and the Poisson's ratio is taken to be constant as $\nu_j = \nu$, $j = 1, 2, 3$, owing to the fact that its variation within a practical range has the rather insignificant influence on the values of the near-tip driving forces for fracture (Ozturk and Erdogan, 1996; Choi, 1997).

With $u_j(x, y)$, $j = x, y$, referring to the displacement components in the x- and y-directions, respectively, a system of governing equations corresponding to Eq. (2) is expressed as

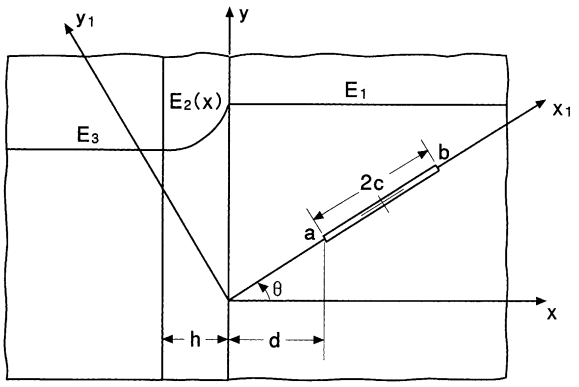

Fig. 1. Schematic representation of bonded half-planes with a crack at an arbitrary angle to the graded interfacial zone.

$$\nabla^2 u_x + \frac{2}{\kappa-1}\frac{\partial}{\partial x}\left(\frac{\partial u_x}{\partial x}+\frac{\partial u_y}{\partial y}\right)+\frac{\beta}{\kappa-1}\left[(1+\kappa)\frac{\partial u_x}{\partial x}+(3-\kappa)\frac{\partial u_y}{\partial y}\right]=0 \tag{4a}$$

$$\nabla^2 u_y + \frac{2}{\kappa-1}\frac{\partial}{\partial y}\left(\frac{\partial u_x}{\partial x}+\frac{\partial u_y}{\partial y}\right)+\beta\left(\frac{\partial u_x}{\partial y}+\frac{\partial u_y}{\partial x}\right)=0 \tag{4b}$$

where $\kappa = (3-4\nu)$ for plane strain and $\kappa = (3-\nu)/(1+\nu)$ for plane stress, and $\beta \neq 0$ for the graded interlayer and $\beta = 0$ for the half-planes.

Using the (x,y) coordinate system, the interface and regularity conditions are written as

$$u_{1x}(0,y) = u_{2x}(0,y),\ \ u_{1y}(0,y) = u_{2y}(0,y);\quad |y|<\infty \tag{5a}$$

$$\sigma_{1xx}(0,y) = \sigma_{2xx}(0,y),\ \ \sigma_{1xy}(0,y) = \sigma_{2xy}(0,y);\quad |y|<\infty \tag{5b}$$

$$u_{2x}(-h,y) = u_{3x}(-h,y),\ \ u_{2y}(-h,y) = u_{3y}(-h,y);\quad |y|<\infty \tag{5c}$$

$$\sigma_{2xx}(-h,y) = \sigma_{3xx}(-h,y),\ \ \sigma_{2xy}(-h,y) = \sigma_{3xy}(-h,y);\quad |y|<\infty \tag{5d}$$

$$u_{ix}(x,y)\to 0,\ \ u_{iy}(x,y)\to 0;\quad i=1,3,\ \ |x|\to\infty \tag{5e}$$

and the mixed conditions along the cracked plane in the (x_1,y_1) coordinate are imposed as

$$\sigma_{1y_1y_1}(x_1,+0) = \sigma_{1y_1y_1}(x_1,-0),\ \ \sigma_{1x_1y_1}(x_1,+0) = \sigma_{1x_1y_1}(x_1,-0);\quad x_1>0 \tag{6a}$$

$$\sigma_{1y_1y_1}(x_1,+0) = p(x_1),\ \ \sigma_{1x_1y_1}(x_1,+0) = q(x_1);\quad a<x_1<b \tag{6b}$$

$$u_{1x_1}(x_1,+0) = u_{1x_1}(x_1,-0),\ \ u_{1y_1}(x_1,+0) = u_{1y_1}(x_1,-0);\quad 0<x_1<a,\ \ x_1>b \tag{6c}$$

where the first numeric subscripts denote the constituent materials, and $p(x_1)$ and $q(x_1)$ describe the arbitrary normal and shear tractions on the crack surface, respectively.

For the cracked half-plane in the right-hand side, the displacements and stresses, u_{1i} and σ_{1ij}, $i,j = x,y$, or $i,j = x_1,y_1$, can be expressed as the sum of two parts derived in the (x,y) coordinate system:

$$u_{1i}(x,y) = u_{1i}^{(1)}(x,y) + u_{1i}^{(2)}(x,y);\quad i=x,y \tag{7a}$$

$$\sigma_{1ij}(x,y) = \sigma_{1ij}^{(1)}(x,y) + \sigma_{1ij}^{(2)}(x,y);\quad i,j=x,y \tag{7b}$$

or in the (x_1,y_1) coordinate system:

$$u_{1i}(x_1,y_1) = u_{1i}^{(1)}(x_1,y_1) + u_{1i}^{(2)}(x_1,y_1);\quad i=x_1,y_1 \tag{8a}$$

$$\sigma_{1ij}(x_1,y_1) = \sigma_{1ij}^{(1)}(x_1,y_1) + \sigma_{1ij}^{(2)}(x_1,y_1);\quad i,j=x_1,y_1 \tag{8b}$$

where the superscript (1) refers to the field components in an infinite plane with a crack and the superscript (2) is for those in the half-plane without the crack.

In order to find the expressions for the field components in the homogeneous full-plane containing a crack along $a<x_1<b$ and $y_1=0$, the general solutions for the displacements in the upper ($y_1>0$) and lower ($y_1<0$) regions are first obtained by solving the governing equations in Eqs. (4a) and (4b) based on the Fourier integral transform method and those for the stresses are obtainable from the constitutive relations. After imposing the traction equilibrium as in Eq. (6a) and defining the unknown auxiliary functions as

$$\phi_1(x_1) = \frac{\partial}{\partial x_1}\left[u^{(1)}_{1y_1}(x_1,+0) - u^{(1)}_{1y_1}(x_1,-0)\right]; \quad x_1 > 0 \tag{9a}$$

$$\phi_2(x_1) = \frac{\partial}{\partial x_1}\left[u^{(1)}_{1x_1}(x_1,+0) - u^{(1)}_{1x_1}(x_1,-0)\right]; \quad x_1 > 0 \tag{9b}$$

the displacements and stresses for the cracked homogeneous full-plane in the (x_1, y_1) coordinate can then be expressed as

$$u^{(1)}_{1x_1}(x_1,y_1) = \frac{1}{2\pi(1+\kappa)}\int_a^b \phi_1(t)\left[(1-\kappa)\ln[y_1^2+(t-x_1)^2]^{1/2} - \frac{2y_1^2}{y_1^2+(t-x_1)^2}\right]\mathrm{d}t - \frac{1}{2\pi}\int_a^b \phi_2(t)\left[\arctan\frac{t-x_1}{y_1} - \frac{2}{1+\kappa}\frac{(t-x_1)y_1}{y_1^2+(t-x_1)^2}\right]\mathrm{d}t \tag{10a}$$

$$u^{(1)}_{1y_1}(x_1,y_1) = -\frac{1}{2\pi}\int_a^b \phi_1(t)\left[\arctan\frac{t-x_1}{y_1} + \frac{2}{1+\kappa}\frac{(t-x_1)y_1}{y_1^2+(t-x_1)^2}\right]\mathrm{d}t - \frac{1}{2\pi(1+\kappa)}\int_a^b \phi_2(t)\left[(1-\kappa)\ln[y_1^2+(t-x_1)^2]^{1/2} + \frac{2y_1^2}{y_1^2+(t-x_1)^2}\right]\mathrm{d}t \tag{10b}$$

$$\sigma^{(1)}_{1x_1x_1}(x_1,y_1) = \frac{2\mu_1}{\pi(1+\kappa)}\int_a^b \phi_1(t)\left[\frac{t-x_1}{y_1^2+(t-x_1)^2} - \frac{2(t-x_1)y_1^2}{[y_1^2+(t-x_1)^2]^2}\right]\mathrm{d}t + \frac{2\mu_1}{\pi(1+\kappa)}\int_a^b \phi_2(t)\left[\frac{2y_1}{y_1^2+(t-x_1)^2} - \frac{y_1[y_1^2-(t-x_1)^2]}{[y_1^2+(t-x_1)^2]^2}\right]\mathrm{d}t \tag{10c}$$

$$\sigma^{(1)}_{1y_1y_1}(x_1,y_1) = \frac{2\mu_1}{\pi(1+\kappa)}\int_a^b \phi_1(t)\left[\frac{t-x_1}{y_1^2+(t-x_1)^2} + \frac{2(t-x_1)y_1^2}{[y_1^2+(t-x_1)^2]^2}\right]\mathrm{d}t + \frac{2\mu_1}{\pi(1+\kappa)}\int_a^b \phi_2(t)\frac{y_1[y_1^2-(t-x_1)^2]}{[y_1^2+(t-x_1)^2]^2}\mathrm{d}t \tag{10d}$$

$$\sigma^{(1)}_{1x_1y_1}(x_1,y_1) = \frac{2\mu_1}{\pi(1+\kappa)}\int_a^b \phi_1(t)\frac{y_1[y_1^2-(t-x_1)^2]}{[y_1^2+(t-x_1)^2]^2}\mathrm{d}t + \frac{2\mu_1}{\pi(1+\kappa)}\int_a^b \phi_2(t)\left[\frac{t-x_1}{y_1^2+(t-x_1)^2} - \frac{2(t-x_1)y_1^2}{[y_1^2+(t-x_1)^2]^2}\right]\mathrm{d}t \tag{10e}$$

where $\mu_1 = E_1/2(1+v)$ is the shear modulus and the functions ϕ_j, $j = 1,2$, are subjected to the following continuity and single-valuedness conditions:

$$\phi_j(x_1) = 0; \quad 0 < x_1 < a, \;\; x_1 > b; \;\; j = 1,2 \tag{11a}$$

$$\int_a^b \phi_j(x_1)\,\mathrm{d}x_1 = 0; \quad j = 1,2 \tag{11b}$$

For the second part of the solutions, the displacement and stress components that satisfy the condition in Eq. (5e) are obtained in the (x, y) coordinate in terms of the Fourier integrals as

$$u_{1x}^{(2)}(x,y) = -\frac{\mathrm{i}}{2\pi}\int_{-\infty}^{\infty}\frac{s}{|s|}\left[G_1 + \left(x + \frac{\kappa}{|s|}\right)G_2\right]\mathrm{e}^{-|s|x-\mathrm{i}sy}\,\mathrm{d}s \tag{12a}$$

$$u_{1y}^{(2)}(x,y) = \frac{1}{2\pi}\int_{-\infty}^{\infty}(G_1 + xG_2)\mathrm{e}^{-|s|x-\mathrm{i}sy}\,\mathrm{d}s \tag{12b}$$

$$\sigma_{1xx}^{(2)}(x,y) = \frac{\mathrm{i}\mu_1}{2\pi}\int_{-\infty}^{\infty}\left[2s(G_1 + xG_2) + \frac{s}{|s|}(1+\kappa)G_2\right]\mathrm{e}^{-|s|x-\mathrm{i}sy}\,\mathrm{d}s \tag{12c}$$

$$\sigma_{1yy}^{(2)}(x,y) = -\frac{\mathrm{i}\mu_1}{2\pi}\int_{-\infty}^{\infty}\left[2s(G_1 + xG_2) - \frac{s}{|s|}(3-\kappa)G_2\right]\mathrm{e}^{-|s|x-\mathrm{i}sy}\,\mathrm{d}s \tag{12d}$$

$$\sigma_{1xy}^{(2)}(x,y) = -\frac{\mu_1}{2\pi}\int_{-\infty}^{\infty}[2|s|(G_1 + xG_2) - (1-\kappa)G_2]\mathrm{e}^{-|s|x-isy}\,\mathrm{d}s \tag{12e}$$

where s is the transform variable, $G_j(s)$, $j = 1, 2$, are arbitrary unknowns to be evaluated, and $i = (-1)^{1/2}$.

The general solutions of displacement and stress components for the nonhomogeneous interlayer with $\beta \neq 0$ are expressed as

$$u_{2x}(x,y) = -\frac{\mathrm{i}}{2\pi}\int_{-\infty}^{\infty}\sum_{j=1}^{4}\lambda_j F_j\,\mathrm{e}^{r_j x-\mathrm{i}sy}\,\mathrm{d}s \tag{13a}$$

$$u_{2y}(x,y) = \frac{1}{2\pi}\int_{-\infty}^{\infty}\sum_{j=1}^{4}F_j\,\mathrm{e}^{r_j x-\mathrm{i}sy}\,\mathrm{d}s \tag{13b}$$

$$\sigma_{2xx}(x,y) = -\frac{\mathrm{i}\mu_2(x)}{2\pi(\kappa-1)}\int_{-\infty}^{\infty}\sum_{j=1}^{4}\left[(1+\kappa)\lambda_j r_j + s(3-\kappa)\right]F_j\,\mathrm{e}^{r_j x-\mathrm{i}sy}\,\mathrm{d}s \tag{13c}$$

$$\sigma_{2yy}(x,y) = -\frac{\mathrm{i}\mu_2(x)}{2\pi(\kappa-1)}\int_{-\infty}^{\infty}\sum_{j=1}^{4}\left[(3-\kappa)\lambda_j r_j + s(1+\kappa)\right]F_j\,\mathrm{e}^{r_j x-\mathrm{i}sy}\,\mathrm{d}s \tag{13d}$$

$$\sigma_{2xy}(x,y) = \frac{\mu_2(x)}{2\pi}\int_{-\infty}^{\infty}\sum_{j=1}^{4}\left(r_j - s\lambda_j\right)F_j\,\mathrm{e}^{r_j x-\mathrm{i}sy}\,\mathrm{d}s \tag{13e}$$

where $\mu_2(x) = E_o\mathrm{e}^{\beta x}/2(1+\nu)$, $F_j(s)$, $j = 1, \ldots, 4$, are arbitrary unknowns, $r_j(s)$, $j = 1, \ldots, 4$, are the roots of the characteristic equation:

$$\left(r^2 + \beta r - s^2\right)^2 + \left(\frac{3-\kappa}{1+\kappa}\right)\beta^2 s^2 = 0 \tag{14}$$

from which the roots are determined as

$$r_j = -\frac{1}{2}\left[\beta - \sqrt{\beta^2 + 4s^2 - (-1)^j 4\beta s\mathrm{i}\left(\frac{3-\kappa}{1+\kappa}\right)^{1/2}}\right]; \quad \mathrm{Re}(r_j) > 0, \;\; j = 1, 2 \tag{15a}$$

$$r_j = -\frac{1}{2}\left[\beta + \sqrt{\beta^2 + 4s^2 + (-1)^j 4\beta s \mathrm{i}\left(\frac{3-\kappa}{1+\kappa}\right)^{1/2}}\right]; \quad \mathrm{Re}(r_j) < 0, \ \ j = 3,4 \tag{15b}$$

and $\lambda_j(s)$, $j = 1,\ldots,4$, are given as

$$\lambda_j = \frac{(\kappa-1)(r_j^2 + \beta r_j) - (\kappa+1)s^2}{[2r_j + (\kappa-1)\beta]s}; \quad j = 1,\ldots,4 \tag{16}$$

For the uncracked half-plane in the left-hand side with $\beta = 0$, the general solutions of displacements and stresses satisfying the regularity condition in Eq. (5e) are also obtained as

$$u_{3x}(x,y) = \frac{\mathrm{i}}{2\pi}\int_{-\infty}^{\infty}\frac{s}{|s|}\left[H_1 + \left(x - \frac{\kappa}{|s|}\right)H_2\right]\mathrm{e}^{|s|x - \mathrm{i}sy}\,\mathrm{d}s \tag{17a}$$

$$u_{3y}(x,y) = \frac{1}{2\pi}\int_{-\infty}^{\infty}(H_1 + xH_2)\mathrm{e}^{|s|x-\mathrm{i}sy}\,\mathrm{d}s \tag{17b}$$

$$\sigma_{3xx}(x,y) = \frac{\mathrm{i}\mu_3}{2\pi}\int_{-\infty}^{\infty}\left[2s(H_1 + xH_2) - \frac{s}{|s|}(1+\kappa)H_2\right]\mathrm{e}^{|s|x-\mathrm{i}sy}\,\mathrm{d}s \tag{17c}$$

$$\sigma_{3yy}(x,y) = -\frac{\mathrm{i}\mu_3}{2\pi}\int_{-\infty}^{\infty}\left[2s(H_1 + xH_2) + \frac{s}{|s|}(3-\kappa)H_2\right]\mathrm{e}^{|s|x-\mathrm{i}sy}\,\mathrm{d}s \tag{17d}$$

$$\sigma_{3xy}(x,y) = \frac{\mu_3}{2\pi}\int_{-\infty}^{\infty}[2|s|(H_1 + xH_2) + (1-\kappa)H_2]\mathrm{e}^{|s|x-\mathrm{i}sy}\,\mathrm{d}s \tag{17e}$$

where $\mu_3 = E_3/2(1+\nu)$ and $H_j(s)$, $j = 1,2$, are arbitrary unknowns.

As noted in the foregoing, the general solutions of the current elasticity equations involve a total of eight arbitrary unknowns, G_j, $j = 1,2$, F_j, $j = 1,\ldots,4$, H_j, $j = 1,2$, and two additional unknown functions ϕ_j, $j = 1,2$. The direct application of interface conditions in Eqs. (5a)–(5d) would lead to a system of equations to be solved for these unknowns in terms of ϕ_j, $j = 1,2$. In what follows, as a systematic way of circumventing the difficulties that may arise from such routine and complicated algebraic manipulations, the stiffness matrix approach is utilized.

3. Stiffness matrix equations for the bonded media

When applying the interface conditions in Eqs. (5a)–(5d), the field components in Eqs. (7a) and (7b) defined in the (x,y) coordinate for the cracked half-plane are to be employed in conjunction with the transformation of the full-plane solutions in Eqs. (10a)–(10e) and using Eqs. (1a) and (1b) such that

$$u_{1x}^{(1)}(x,y) = m u_{1x_1}^{(1)}(x_1,y_1) - n u_{1y_1}^{(1)}(x_1,y_1) \tag{18a}$$

$$u_{1y}^{(1)}(x,y) = n u_{1x_1}^{(1)}(x_1,y_1) + m u_{1y_1}^{(1)}(x_1,y_1) \tag{18b}$$

$$\sigma_{1xx}^{(1)}(x,y) = m^2\sigma_{1x_1x_1}^{(1)}(x_1,y_1) - 2mn\sigma_{1x_1y_1}^{(1)}(x_1,y_1) + n^2\sigma_{1y_1y_1}^{(1)}(x_1,y_1) \tag{18c}$$

$$\sigma_{1xy}^{(1)}(x,y) = mn\left[\sigma_{1x_1x_1}^{(1)}(x_1,y_1) - \sigma_{1y_1y_1}^{(1)}(x_1,y_1)\right] + \left(m^2 - n^2\right)\sigma_{1x_1y_1}^{(1)}(x_1,y_1) \tag{18d}$$

The displacement and stress vectors are then defined in the transformed domain (x,s) as

$$\bar{\boldsymbol{d}}_j(x,s)=\{-i\bar{u}_{jx}\ \ \bar{u}_{jy}\},\ \ \bar{\boldsymbol{\sigma}}_j(x,s)=\{-i\bar{\sigma}_{jxx}\ \ \bar{\sigma}_{jxy}\};\quad j=1,2,3 \tag{19}$$

and the displacements $\bar{\boldsymbol{d}}_j^{\mp}(s)$ and the tractions $\bar{\boldsymbol{\sigma}}_j^{\mp}(s)$ evaluated at the left- $(-)$ and right-hand side $(+)$ surfaces for each of the constituents are, respectively, expressed in matrix form in terms of the corresponding unknowns, G_j, $j=1,2$, F_j, $j=1,\ldots,4$, and H_j, $j=1,2$. Upon eliminating the unknowns from these two separate matrix equations for each constituent, the relationship between the values of $\bar{\boldsymbol{d}}_j^{\mp}(s)$ and $\bar{\boldsymbol{\sigma}}_j^{\mp}(s)$, $j=1,2,3$, can be obtained as

$$-\bar{\boldsymbol{\sigma}}_1^{-}=\boldsymbol{K}_{22}^{(1)}\bar{\boldsymbol{d}}_1^{-}-\boldsymbol{f}_0 \tag{20a}$$

$$\left\{\begin{array}{c}\bar{\boldsymbol{\sigma}}_2^{+}\\ \hdashline -\bar{\boldsymbol{\sigma}}_2^{-}\end{array}\right\}=\left[\begin{array}{c:c}\boldsymbol{K}_{11}^{(2)} & \boldsymbol{K}_{12}^{(2)}\\ \hdashline \boldsymbol{K}_{21}^{(2)} & \boldsymbol{K}_{22}^{(2)}\end{array}\right]\left\{\begin{array}{c}\bar{\boldsymbol{d}}_2^{+}\\ \hdashline \bar{\boldsymbol{d}}_2^{-}\end{array}\right\} \tag{20b}$$

$$\bar{\boldsymbol{\sigma}}_3^{+}=\boldsymbol{K}_{11}^{(3)}\bar{\boldsymbol{d}}_3^{+} \tag{20c}$$

where $\boldsymbol{K}_{ij}^{(2)}(s)$, $i,j=1,2$, are 2×2 submatrices of the 4×4 symmetric local stiffness matrix for the graded interlayer, $\boldsymbol{K}_{22}^{(1)}(s)$ and $\boldsymbol{K}_{11}^{(3)}(s)$ are the 2×2 symmetric local stiffness matrices for the semi-infinite constituents 1 and 3, and the vector $\boldsymbol{f}_{\mathrm{o}}(s)=\{f_{\mathrm{o}1}\ \ f_{\mathrm{o}2}\}$ is given as

$$\left\{\begin{array}{c}f_{\mathrm{o}1}(s)\\ f_{\mathrm{o}2}(s)\end{array}\right\}=\frac{\mu_1}{\kappa}\left[\begin{array}{cc}|s|(1+\kappa) & s(1-\kappa)\\ s(1-\kappa) & |s|(1+\kappa)\end{array}\right]\left\{\begin{array}{c}g_1\\ g_2\end{array}\right\}-\frac{2\mu_1}{1+\kappa}\left\{\begin{array}{c}g_3\\ g_4\end{array}\right\} \tag{21}$$

in which $g_j(s)$, $j=1,\ldots,4$, are the functions obtained by taking the Fourier transform of the full-plane solutions at $x=0$ with respect to y-axis to be written in terms of ϕ_j, $j=1,2$, as

$$\begin{aligned}g_1(s)=&\int_a^b\phi_1(t)\left[\frac{\mathrm{i}m}{1+\kappa}\left(\frac{1-\kappa}{2|s|}-mt\right)-\frac{n}{s}\left(\frac{1}{2}+\frac{mt|s|}{1+\kappa}\right)\right]\mathrm{e}^{-|s|mt+\mathrm{i}snt}\,\mathrm{d}t\\&+\int_a^b\phi_2(t)\left[\frac{\mathrm{i}n}{1+\kappa}\left(\frac{1-\kappa}{2|s|}-mt\right)+\frac{m}{s}\left(\frac{1}{2}+\frac{mt|s|}{1+\kappa}\right)\right]\mathrm{e}^{-|s|mt+\mathrm{i}snt}\,\mathrm{d}t\end{aligned} \tag{22a}$$

$$\begin{aligned}g_2(s)=&\int_a^b\phi_1(t)\left[\frac{\mathrm{i}m}{s}\left(\frac{1}{2}-\frac{mt|s|}{1+\kappa}\right)-\frac{n}{1+\kappa}\left(\frac{1-\kappa}{2|s|}+mt\right)\right]\mathrm{e}^{-|s|mt+\mathrm{i}snt}\,\mathrm{d}t\\&+\int_a^b\phi_2(t)\left[\frac{\mathrm{i}n}{s}\left(\frac{1}{2}-\frac{mt|s|}{1+\kappa}\right)+\frac{m}{1+\kappa}\left(\frac{1-\kappa}{2|s|}+mt\right)\right]\mathrm{e}^{-|s|mt+\mathrm{i}snt}\,\mathrm{d}t\end{aligned} \tag{22b}$$

$$\begin{aligned}g_3(s)=&\int_a^b\phi_1(t)\left[\mathrm{i}m^2|s|t+\frac{ns}{|s|}(1+m|s|t)\right]\mathrm{e}^{-|s|mt+\mathrm{i}snt}\,\mathrm{d}t\\&+\int_a^b\phi_2(t)\left[\mathrm{i}mn|s|t-\frac{ms}{|s|}(1+m|s|t)\right]\mathrm{e}^{-|s|mt+\mathrm{i}snt}\,\mathrm{d}t\end{aligned} \tag{22c}$$

$$\begin{aligned}g_4(s)=&\int_a^b\phi_1(t)\left[\frac{\mathrm{i}ms}{|s|}(m|s|t-1)+mn|s|t\right]\mathrm{e}^{-|s|mt+\mathrm{i}snt}\,\mathrm{d}t\\&+\int_a^b\phi_2(t)\left[\frac{\mathrm{i}ns}{|s|}(m|s|t-1)-m^2|s|t\right]\mathrm{e}^{-|s|mt+\mathrm{i}snt}\,\mathrm{d}t\end{aligned} \tag{22d}$$

It is noted that the imaginary part of the local stiffness matrix for the nonhomogeneous graded interlayer is a null matrix as

$$\operatorname{Im} \boldsymbol{K}_{ij}^{(2)}(s) = \boldsymbol{0} \tag{23}$$

and the following asymptotic behavior holds for the constituent materials

$$\lim_{s\to\infty} \frac{1}{s} \boldsymbol{K}_{ij}^{(k)}(s) = \begin{cases} \boldsymbol{K}_{ii\infty}^{(k)}; & i = j, \ k = 1,2,3 \\ \boldsymbol{0}; & i \neq j, \ k = 1,2,3 \end{cases} \tag{24}$$

where $\boldsymbol{K}_{ii\infty}^{(k)}$ are the 2×2 real and symmetric submatrices containing limiting nonzero values.

By defining $\overline{\boldsymbol{\delta}}_j(s) \equiv \bar{\boldsymbol{d}}_j^-(s) = \bar{\boldsymbol{d}}_{j+1}^+(s)$, $j = 1,2$, as vectors for the interfacial displacements common to the adjacent constituents and assembling the local stiffness matrix equations in Eqs. (20a)–(20c) via the interface continuity conditions in Eqs. (5a)–(5d), a system of global stiffness matrix equations is constructed with $\overline{\boldsymbol{\delta}}_j$, $j = 1,2$, as the basic unknown variables:

$$\left[\begin{array}{c:c} \boldsymbol{K}_{22}^{(1)} + \boldsymbol{K}_{11}^{(2)} & \boldsymbol{K}_{12}^{(2)} \\ \hdashline \boldsymbol{K}_{21}^{(2)} & \boldsymbol{K}_{22}^{(2)} + \boldsymbol{K}_{11}^{(3)} \end{array}\right] \left\{\begin{array}{c} \overline{\boldsymbol{\delta}}_1 \\ \hdashline \overline{\boldsymbol{\delta}}_2 \end{array}\right\} = \left\{\begin{array}{c} \boldsymbol{f}_{\mathrm{o}} \\ \hdashline \boldsymbol{0} \end{array}\right\} \tag{25}$$

or in brief, the above system of algebraic equations is expressed as

$$\boldsymbol{K}\overline{\boldsymbol{\delta}} = \boldsymbol{f} \tag{26}$$

where $\boldsymbol{K}(s)$ is a 4×4 symmetric global stiffness matrix, $\overline{\boldsymbol{\delta}}(s) = \{\overline{\boldsymbol{\delta}}_1 \ \ \overline{\boldsymbol{\delta}}_2\}$ is a global vector for the interfacial displacements, and $\boldsymbol{f}(s) = \{\boldsymbol{f}_{\mathrm{o}} \ \ \boldsymbol{0}\}$ is a vector containing the auxiliary functions ϕ_j, $j = 1,2$, and zero elements.

Upon solving the global stiffness matrix equations for the global interfacial displacements $\overline{\boldsymbol{\delta}}$, the expressions for the required unknowns, G_j, $j = 1,2$, F_j, $j = 1,\ldots,4$, and H_j, $j = 1,2$, that satisfy the interfacial conditions can readily be obtained from the relations between these unknowns and the local interfacial displacements, $\overline{\boldsymbol{\delta}}_j$, $j = 1,2$. The auxiliary functions ϕ_j, $j = 1,2$, thus become the only unknowns to be determined from the crack surface condition in Eq. (6b).

4. Derivation of singular integral equations

In order to apply the remaining crack surface condition defined in the (x_1, y_1) coordinate, the traction components in Eq. (8b) for the cracked half-plane are used with the transformation of the second part of its solutions in Eqs. (12c)–(12e) as

$$\sigma_{1y_1y_1}^{(2)}(x_1,y_1) = n^2\sigma_{1xx}^{(2)}(x,y) - 2mn\sigma_{1xy}^{(2)}(x,y) + m^2\sigma_{1yy}^{(2)}(x,y) \tag{27a}$$

$$\sigma_{1x_1y_1}^{(2)}(x_1,y_1) = mn\left[\sigma_{1yy}^{(2)}(x,y) - \sigma_{1xx}^{(2)}(x,y)\right] + \left(m^2 - n^2\right)\sigma_{1xy}^{(2)}(x,y) \tag{27b}$$

$$x = mx_1 - ny_1, \quad y = nx_1 + my_1 \tag{27c}$$

so that the tractions along the cracked plane, $y_1 = 0$ and $x_1 > 0$, are expressed as

$$\frac{\pi}{2\mu_1}\lim_{y_1\to+0}\sigma_{1y_1y_1}(x_1,y_1)=\frac{1}{1+\kappa}\int_a^b\frac{\phi_1(t)}{t-x_1}\,\mathrm{d}t+mn\int_{-\infty}^{\infty}\left[|s|G_1+\left(|s|mx_1-\frac{1}{2}+\frac{\kappa}{2}\right)G_2\right]\mathrm{e}^{-(|s|m+\mathrm{i}sn)x_1}\,\mathrm{d}s$$
$$+\frac{\mathrm{i}}{2}\int_{-\infty}^{\infty}\left\{\left(n^2-m^2\right)\left[sG_1+\left(smx_1+\frac{s}{|s|}\frac{\kappa}{2}\right)G_2\right]\right.$$
$$\left.+\frac{s}{|s|}\left(\frac{1}{2}+m^2\right)G_2\right\}\mathrm{e}^{-(|s|m+\mathrm{i}sn)x_1}\,\mathrm{d}s \tag{28a}$$

$$\frac{\pi}{2\mu_1}\lim_{y_1\to+0}\sigma_{1x_1y_1}(x_1,y_1)=\frac{1}{1+\kappa}\int_a^b\frac{\phi_2(t)}{t-x_1}\,\mathrm{d}t+\frac{1}{2}\left(n^2-m^2\right)\int_{-\infty}^{\infty}\left[|s|G_1+\left(|s|mx_1-\frac{1}{2}+\frac{\kappa}{2}\right)G_2\right]\mathrm{e}^{-(|s|m+\mathrm{i}sn)x_1}\,\mathrm{d}s$$
$$-\mathrm{i}mn\int_{-\infty}^{\infty}\left\{sG_1+\left[smx_1+\frac{s}{|s|}\frac{(\kappa-1)}{2}\right]G_2\right\}\mathrm{e}^{-(|s|m+\mathrm{i}sn)x_1}\,\mathrm{d}s \tag{28b}$$

where the first terms in the right-hand side contain the Cauchy singular kernel $1/(t-x_1)$ and the expressions for the unknowns G_j, $j=1,2$, are obtained as outlined above in the form as

$$G_1(s)=\mu_1\sum_{j=1}^{2}\left[\frac{1}{\kappa}L_{2j-1}g_j-\frac{2}{1+\kappa}L_{2j+3}g_{j+2}\right] \tag{29a}$$

$$G_2(s)=\frac{\mu_1}{\kappa}\sum_{j=1}^{2}\left[\frac{1}{\kappa}L_{2j}g_j-\frac{2}{1+\kappa}L_{2j+4}g_{j+2}\right] \tag{29b}$$

in which the functions $L_j(s)$, $j=1,\ldots,8$, are defined as

$$L_1(s)=s\left[\frac{|s|}{s}(1+\kappa)F_{12}+(1-\kappa)F_{22}\right] \tag{30a}$$

$$L_2(s)=-s\left[|s|(1+\kappa)F_{11}+2sF_{12}+|s|(1-\kappa)F_{22}-\frac{\kappa}{\mu_1}\right] \tag{30b}$$

$$L_3(s)=s\left[(1-\kappa)F_{12}+\frac{|s|}{s}(1+\kappa)F_{22}-\frac{\kappa}{s\mu_1}\right] \tag{30c}$$

$$L_4(s)=-s\left[s(1-\kappa)F_{11}+2|s|F_{12}+s(1+\kappa)F_{22}-\frac{|s|}{s}\frac{\kappa}{\mu_1}\right] \tag{30d}$$

$$L_5(s)=F_{12},\quad L_6(s)=-(sF_{11}+|s|F_{12}) \tag{30e}$$

$$L_7(s)=F_{22},\quad L_8(s)=-(sF_{12}+|s|F_{22}) \tag{30f}$$

with $F_{ij}(s)$, $i,j=1,\ldots,4$, denoting the elements of the global flexibility matrix as $\boldsymbol{F}(s)\equiv\boldsymbol{K}^{-1}(s)$.

After substituting Eqs. (29a) and (29b) into Eqs. (28a) and (28b) followed by some algebraic manipulations and applying the crack surface condition in Eq. (6b), a system of singular integral equations with a Cauchy kernel is derived as

$$\int_a^b\frac{\phi_1(t)}{t-x_1}\,\mathrm{d}t+\int_a^b\sum_{j=1}^{2}k_{1j}(x_1,t)\phi_j(t)\,\mathrm{d}t=\frac{\pi(1+\kappa)}{2\mu_1}p(x_1);\quad a\leqslant x_1\leqslant b \tag{31a}$$

$$\int_a^b \frac{\phi_2(t)}{t-x_1}\,\mathrm{d}t + \int_a^b \sum_{j=1}^{2} k_{2j}(x_1,t)\phi_j(t)\,\mathrm{d}t = \frac{\pi(1+\kappa)}{2\mu_1} q(x_1); \quad a \leqslant x_1 \leqslant b \tag{31b}$$

where the kernels $k_{ij}(x_1,t)$, $i,j=1,2$, are, upon separating the even and odd properties in s from the relevant expressions, obtained as

$$k_{ij}(x_1,t) = \int_0^\infty \left[\Lambda_{ij}(s,x_1,t)\cos sn(t-x_1) - \Lambda_{i(j+2)}(s,x_1,t)\sin sn(t-x_1)\right]\mathrm{e}^{-sm(t+x_1)}\,\mathrm{d}s; \quad i,j=1,2 \tag{32}$$

in which the integrands $\Lambda_{ij}(s,x_1,t)$, $i=1,2$, $j=1,\ldots,4$, are written as

$$\begin{aligned}\Lambda_{i1}(s,x_1,t) = -\frac{\mu_1}{2\kappa}\Bigg[&\frac{n}{s}(1+\kappa+2mts)M_{i1}(s,x_1) + m\left(\frac{1-\kappa}{s}-2mt\right)M_{i2}(s,x_1) + n\left(\frac{1-\kappa}{s}+2mt\right)M_{i3}(s,x_1)\\ &+\frac{m}{s}(1+\kappa-2mts)M_{i4}(s,x_1)\Bigg] - 2\mu_1\big[n(1+mts)M_{i5}(s,x_1) - m^2 tsM_{i6}(s,x_1)\\ &+ mntsM_{i7}(s,x_1) + m(1-mts)M_{i8}(s,x_1)\big]\end{aligned} \tag{33a}$$

$$\begin{aligned}\Lambda_{i2}(s,x_1,t) = \frac{\mu_1}{2\kappa}\Bigg[&\frac{m}{s}(1+\kappa+2mts)M_{i1}(s,x_1) - n\left(\frac{1-\kappa}{s}-2mt\right)M_{i2}(s,x_1) + m\left(\frac{1-\kappa}{s}+2mt\right)M_{i3}(s,x_1)\\ &-\frac{n}{s}(1+\kappa-2mts)M_{i4}(s,x_1)\Bigg] + 2\mu_1\big[m(1+mts)M_{i5}(s,x_1) + mntsM_{i6}(s,x_1) + m^2 tsM_{i7}(s,x_1)\\ &- n(1-mts)M_{i8}(s,x_1)\big]\end{aligned} \tag{33b}$$

$$\begin{aligned}\Lambda_{i3}(s,x_1,t) = \frac{\mu_1}{2\kappa}\Bigg[&m\left(\frac{1-\kappa}{s}-2mt\right)M_{i1}(s,x_1) - \frac{n}{s}(1+\kappa+2mts)M_{i2}(s,x_1) + \frac{m}{s}(1+\kappa-2mts)M_{i3}(s,x_1)\\ &- n\left(\frac{1-\kappa}{s}+2mt\right)M_{i4}(s,x_1)\Bigg] - 2\mu_1\big[m^2 tsM_{i5}(s,x_1) + n(1+mts)M_{i6}(s,x_1)\\ &- m(1-mts)M_{i7}(s,x_1) + mntsM_{i8}(s,x_1)\big]\end{aligned} \tag{33c}$$

$$\begin{aligned}\Lambda_{i4}(s,x_1,t) = \frac{\mu_1}{2\kappa}\Bigg[&n\left(\frac{1-\kappa}{s}-2mt\right)M_{i1}(s,x_1) + \frac{m}{s}(1+\kappa+2mts)M_{i2}(s,x_1) + \frac{n}{s}(1+\kappa-2mts)M_{i3}(s,x_1)\\ &+ m\left(\frac{1-\kappa}{s}+2mt\right)M_{i4}(s,x_1)\Bigg] - 2\mu_1\big[mntsM_{i5}(s,x_1) - m(1+mts)M_{i6}(s,x_1)\\ &- n(1-mts)M_{i7}(s,x_1) - m^2 tsM_{i8}(s,x_1)\big]; \quad i=1,2\end{aligned} \tag{33d}$$

together with the expressions for $M_{ij}(s,x_1)$, $i=1,2$, $j=1,\ldots,8$, as

$$M_{1j}(s,x_1) = mn\left[2sL_j + \frac{1}{\kappa}(\kappa-1+2mx_1 s)L_{j+1}\right]; \quad j=1,3,5,7 \tag{34a}$$

$$M_{1j}(s,x_1) = \left(n^2-m^2\right)\left[sL_{j-1} + \frac{1}{\kappa}\left(\frac{\kappa-1}{2}+mx_1 s\right)L_j\right] + \frac{L_j}{\kappa}; \quad j=2,4,6,8 \tag{34b}$$

$$M_{2j}(s,x_1) = \left(n^2-m^2\right)\left[sL_j + \frac{1}{\kappa}\left(\frac{\kappa-1}{2}+mx_1 s\right)L_{j+1}\right]; \quad j=1,3,5,7 \tag{34c}$$

$$M_{2j}(s,x_1) = -mn\left[2sL_{j-1} + \frac{1}{\kappa}(\kappa - 1 + 2mx_1 s)L_j\right]; \quad j = 2,4,6,8 \tag{34d}$$

It should be mentioned that the integrands in Eqs. (33a)–(33d) possess the following asymptotic behavior for large values of s such that

$$\lim_{s\to\infty} \Lambda_{ij}(s,x_1,t)\mathrm{e}^{-sm(t+x_1)} = 0; \quad a < (x_1,t) < b, \;\; 0 \leqslant m \leqslant 1 \tag{35}$$

implying that the kernels $k_{ij}(x_1,t)$, $i, j = 1,2$, in Eq. (32) are bounded. To be noted from the above is the disappearance of the exponential decay when $\theta \to 90^\circ$ or $(t + x_1) \to 0.0$, rendering the convergence of the related infinite integrals relatively slow than otherwise. The former corresponds to a crack lying along or parallel to the nominal interface with the graded interlayer, while the latter is for a crack that has one of its tips terminating at the interface. Besides, for a crack with its location specified as $d = 0.0$ and $0^\circ \leqslant \theta \leqslant 90^\circ$, it can be shown that the kernels contain the logarithmic singularities which are, however, square integrable so that they can be treated as part of the regular kernels in the presence of the Cauchy singularities $1/(t - x_1)$. Thus, the near-tip singular stress field would remain to be standard square-root type, provided the elastic properties are continuous and not necessarily differentiable at and in the immediate vicinity of the crack tip, independent of the crack orientation as described by Erdogan et al. (1991) and Ozturk and Erdogan (1996) for the two limiting cases of $\theta = 0^\circ$ and $\theta = 90^\circ$, respectively. These features are in contrast to the dependence of the order of crack-tip stress singularity on both the elastic constants of the constituents and the angle at which the crack intersects the bimaterial interface of zero thickness in piecewise homogeneous bonded media (Bogy, 1971).

5. Solution of integral equations and stress intensity factors

With the dominant singular kernel yet attributed only to the Cauchy type for $d = 0.0$ as well as $d > 0.0$, the square-root crack-tip behavior is retained for the inclined crack geometry. As a result, the auxiliary functions ϕ_j, $j = 1,2$, can be expressed as (Muskhelishvili, 1953)

$$\phi_j(t) = \frac{h_j(t)}{\sqrt{(t-a)(b-t)}}; \quad a < t < b, \;\; j = 1,2 \tag{36}$$

where $h_j(t)$, $j = 1,2$, are unknown functions bounded and nonzero at $t = a$ and $t = b$, and in the normalized interval

$$\begin{Bmatrix} x_1 \\ t \end{Bmatrix} = \frac{b-a}{2}\begin{Bmatrix} \xi \\ \eta \end{Bmatrix} + \frac{b+a}{2}; \quad -1 < (\xi,\eta) < 1 \tag{37}$$

the solutions to the system of singular integral equations can be determined by expanding them into the series of the Chebyshev polynomials of the first kind T_n as

$$\phi_j(t) = \phi_j(\eta) = \frac{1}{\sqrt{1-\eta^2}}\sum_{n=0}^{\infty} c_{jn}T_n(\eta); \quad |\eta| < 1, \;\; j = 1,2 \tag{38}$$

in which c_{jn}, $j = 1,2$, $n \geqslant 0$, are the coefficients to be evaluated. It is noted that $c_{j0} = 0$, $j = 1,2$, and the orthogonality of T_n can be used to satisfy the compatibility condition in Eq. (11b):

$$\int_{-1}^{1} \phi_j(\eta)\,\mathrm{d}\eta; \quad j = 1,2 \tag{39}$$

After substituting from Eqs. (36)–(38) into Eqs. (31a) and (31b), truncated with the first N terms, and using the properties of the Chebyshev polynomial (Gradshteyn and Ryzhik, 1980), the singular integral equations are regularized as

$$\pi\sum_{n=1}^{N}c_{in}U_{n-1}(\xi)+\frac{b-a}{2}\sum_{n=1}^{N}\sum_{j=1}^{2}c_{jn}H_{ij}^{n}(\xi)=f_i(\xi);\quad |\xi|<1,\ \ i=1,2 \tag{40}$$

where U_n is the Chebyshev polynomial of the second kind and the functions $H_{ij}^{n}(\xi)$ and $f_i(\xi)$ are defined as

$$H_{ij}^{n}(\xi)=\int_{-1}^{1}\frac{k_{ij}(\xi,\eta)T_n(\eta)}{\sqrt{1-\eta^2}}\,\mathrm{d}\eta;\quad i,j=1,2 \tag{41a}$$

$$f_1(\xi)=\frac{\pi(1+\kappa)}{2\mu_1}p(\xi),\quad f_2(\xi)=\frac{\pi(1+\kappa)}{2\mu_1}q(\xi) \tag{41b}$$

To recast the functional equations in Eq. (40) into a linear system of $2N$ algebraic equations for the unknown coefficients c_{jn}, $j=1,2$, $1\leqslant n\leqslant N$, the collocation technique can be applied (Erdogan, 1978). The zeros of T_N are employed as a set of collocation points which are concentrated near the ends $\xi=\pm1$ such that

$$T_N(\xi_i)=0,\ \ \xi_i=\cos\left[\frac{\pi(2i-1)}{2N}\right];\quad i=1,2,\ldots,N \tag{42}$$

The important problem in the numerical analysis is the evaluation of the kernels $k_{ij}(x_1,t)$, $i,j=1,2$, in Eq. (32) involving the infinite integrations. To this end, the rate of decay of the integrands with respect to the variable s is to be first examined in order to determine the value of $s=s_{\max}$ at which the values of the integrands become negligibly small. The upper limit of integration is thus taken to be finite but sufficiently large, rather than $s=\infty$. Subsequently, the interval $[0,s_{\max}]$ is divided into a number of subintervals of variable width on the basis of the functional dependence of the integrands upon the variation of the argument. The subintervals are mapped onto the unit intervals $[+1,-1]$ with the Gauss–Legendre quadrature being applied on each mapped subinterval. The values of the kernels are then obtained by summing up the individual contributions from the subintervals. To be also mentioned is that the integrals $H_{ij}^{n}(\xi)$ in Eq. (41a) are of Gauss–Chebyshev type and can readily be evaluated by using the corresponding quadrature formula (Davis and Rabinowitz, 1984). In addition, the number of terms and collocation points N in Eqs. (40) and (42) must be large enough for the solution to converge to a desired degree of accuracy.

Once the values of c_{jn}, $j=1,2$, $1\leqslant n\leqslant N$, are calculated as described in the foregoing, the integral equations in Eqs. (31a) and (31b) provide the dominant singular tractions, $\sigma_{1y_1y_1}(\xi,0)$ and $\sigma_{1x_1y_1}(\xi,0)$, ahead of the crack tips $|\xi|>1$ as

$$\left\{\begin{array}{c}\sigma_{1y_1y_1}(\xi,0)\\ \sigma_{1x_1y_1}(\xi,0)\end{array}\right\}=-\frac{2\mu_1}{1+\kappa}\sum_{n=1}^{N}\left\{\begin{array}{c}c_{1n}\\ c_{2n}\end{array}\right\}\frac{\left[\xi-\mathrm{sgn}(\xi)\sqrt{\xi^2-1}\right]^n}{\mathrm{sgn}(\xi)\sqrt{\xi^2-1}}+\mathrm{O}(1);\quad |\xi|>1 \tag{43}$$

where $\mathrm{O}(\cdot)$ denotes the nonsingular terms and due to the elastic property continuity through the interlayer, the stresses are also continuous at the location of interface with the interlayer.

As physical parameters of primary significance in quantifying the local crack-tip behavior in linear elastic fracture mechanics, the mixed-mode stress intensity factors are defined as

$$\left\{\begin{array}{c}K_{\mathrm{I}}(a)\\ K_{\mathrm{II}}(a)\end{array}\right\}=\lim_{x_1\to a}\sqrt{2(a-x_1)}\left\{\begin{array}{c}\sigma_{1y_1y_1}(x_1,0)\\ \sigma_{1x_1y_1}(x_1,0)\end{array}\right\};\quad x_1<a \tag{44a}$$

$$\left\{ \begin{array}{c} K_{\mathrm{I}}(b) \\ K_{\mathrm{II}}(b) \end{array} \right\} = \lim_{x_1 \to b} \sqrt{2(x_1 - b)} \left\{ \begin{array}{c} \sigma_{1y_1y_1}(x_1, 0) \\ \sigma_{1x_1y_1}(x_1, 0) \end{array} \right\}; \quad x_1 > b \tag{44b}$$

where K_{I} and K_{II} are the modes I and II stress intensity factors, respectively, which by using Eqs. (43) and (37), can be evaluated in terms of the solutions to the integral equations as

$$\left\{ \begin{array}{c} K_{\mathrm{I}}(a) \\ K_{\mathrm{II}}(a) \end{array} \right\} = \frac{2\mu_1}{1+\kappa} \sqrt{\frac{b-a}{2}} \sum_{n=1}^{N} (-1)^n \left\{ \begin{array}{c} c_{1n} \\ c_{2n} \end{array} \right\} \tag{45a}$$

$$\left\{ \begin{array}{c} K_{\mathrm{I}}(b) \\ K_{\mathrm{II}}(b) \end{array} \right\} = -\frac{2\mu_1}{1+\kappa} \sqrt{\frac{b-a}{2}} \sum_{n=1}^{N} \left\{ \begin{array}{c} c_{1n} \\ c_{2n} \end{array} \right\} \tag{45b}$$

in which the continuity of stress components at the nominal interface renders the defined stress intensity factors equally valid even for the limiting case of $d = 0.0$ as well.

6. Results and discussion

The numerical results are obtained as a function of the crack orientation angle θ for various combinations of material $(\beta c, E_3/E_1)$ and geometric $(\theta, h/2c, d/c)$ parameters of the bonded media, with the Poisson's ratio $v = 0.3$. Both the uniform crack surface tractions and the remote biaxial stresses are considered as the external loading conditions under the state of plane strain. In generating the numerical results, it was noted that the convergence rate of the kernels, in general, decreases with the decreasing interlayer thickness h and crack distance d and with the increasing crack angle θ. The adequate range of integration for evaluating the related infinite integrals was found to be $[0, s_{\max}] = [0, 80]$, which was divided into 61 subintervals of incremental width, with 10 integration points allocated in each mapped subinterval. Besides, the number of Gauss–Chebyshev integration points and that of expansion terms and collocation points N in Eqs. (40) and (42) were increased until the values of stress intensity factors converge. The largest number used was $N = 30$. It was checked out that the outlined numerical scheme is sufficient to obtain roughly three-digit accuracy beyond the decimal point for the material and geometric configurations presented in this study. Consequently, neither increasing the number of integration or collocation points nor extending the range of integration had an appreciable effect on the results.

6.1. Uniform normal and shear tractions on the crack surface

To confirm the validity of the analytical procedure and numerical results to be examined henceforth, the values of stress intensity factors for the two special crack orientations, $\theta = 0°$ and $\theta = 90°$, are first presented in Figs. 3 and 4 as a function of interlayer thickness, $h/2c$, for some values of dimensionless nonhomogeneity parameter βc. For a crack impinging upon the interface with the graded interlayer at an angle $\theta = 0°$ and $d/c = 0.0$, the variations of uncoupled and normalized modes I and II stress intensity factors due to the uniform normal ($p = -\sigma_o$, $q = 0$ in Eq. (6b)) and shear ($p = 0$, $q = -\tau_o$ in Eq. (6b)) tractions on the crack surface (Fig. 2) are shown in Fig. 3a and b, respectively, where the relative increases in the stiffness of the nearby half-plane $(x < 0)$ for negative βc tend to reduce the stress intensity factors. For comparison purposes, the results for $h/2c = \infty$ obtained by Erdogan et al. (1991) and the author for the modes I and II crack, respectively, are added by solid circles. When $\theta = 90°$ and $d/c = 0.0$ for which the problem becomes that of a mixed-mode interface crack, the results are illustrated in Fig. 4a and b, subjected to modes I and II loading, respectively. It is then observed that as βc increases, owing to the overall reduction in the stiffness of the plane, the major components of stress intensity factors (i.e., K_{I} under mode I loading and K_{II} under

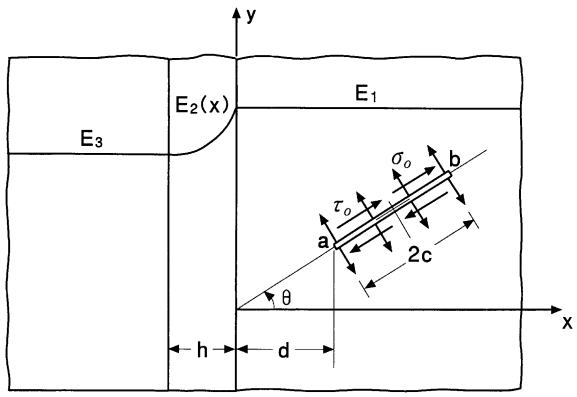

Fig. 2. Bonded half-planes with a graded interfacial zone and an inclined crack subjected to uniform normal (mode I) and uniform shear (mode II) tractions on the crack surface.

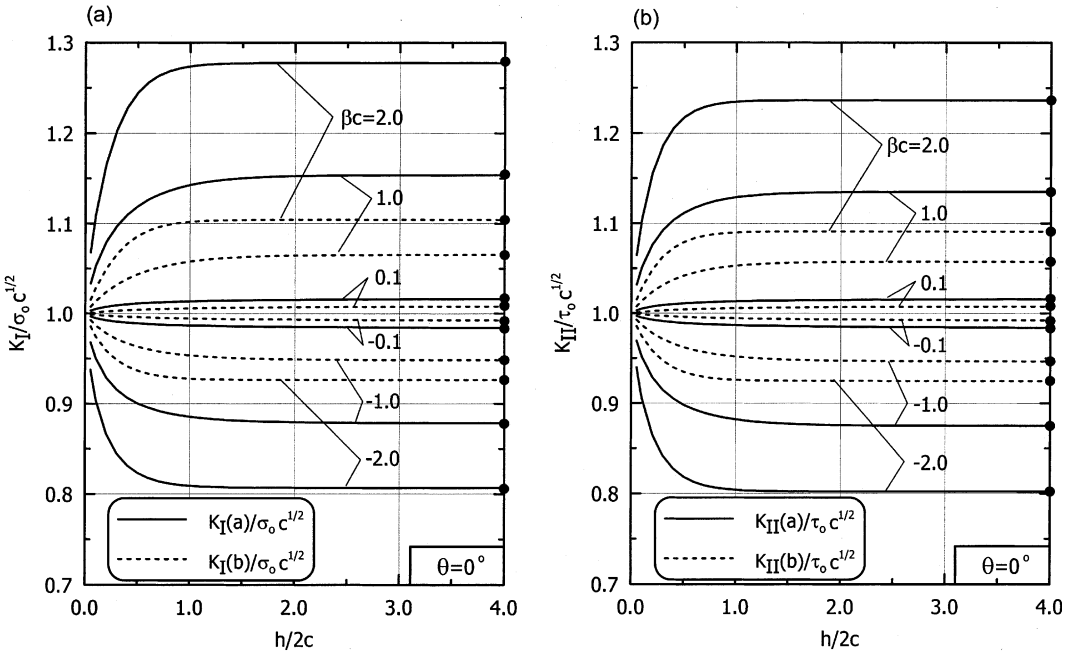

Fig. 3. Single-mode stress intensity factors: (a) $K_{\mathrm{I}}/\sigma_{\mathrm{o}}c^{1/2}$ under mode I loading ($p=-\sigma_{\mathrm{o}}$ and $q=0$); (b) $K_{\mathrm{II}}/\tau_{\mathrm{o}}c^{1/2}$ under mode II loading ($p=0$ and $q=-\tau_{\mathrm{o}}$) for a perpendicular crack as a function of graded interlayer thickness $h/2c$ for different values of non-homogeneity parameter βc ($\theta=0^{\circ}$ and $d/c=0.0$).

mode II loading) increase, while the coupling stress intensity factors (i.e., K_{I} under mode II loading and K_{II} under mode I loading), which are considerably smaller than the major ones, become negligible as βc tends to zero. Also plotted by solid circles in this case are those for $h/2c=\infty$ given by Chen (1990). For these two crack orientations and fixed values of βc, as the thickness ratio $h/2c$ increases, the present solutions approach the preexisting ones rapidly to be in close agreement when $h/2c>2.0$ substantiating the general accuracy of the solutions, although the results for the homogeneous medium are being recovered when $h/2c$

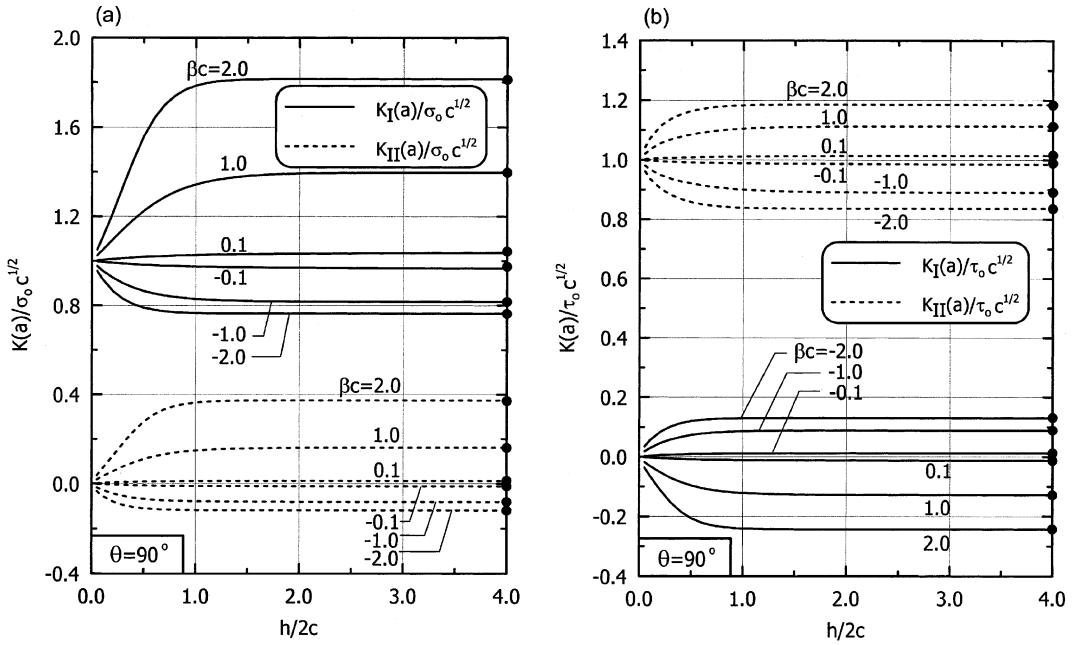

Fig. 4. Mixed-mode stress intensity factors: (a) $[K_{\mathrm{I}}, K_{\mathrm{II}}]/\sigma_{\mathrm{o}}c^{1/2}$ under mode I loading ($p = -\sigma_{\mathrm{o}}$ and $q = 0$); (b) $[K_{\mathrm{I}}, K_{\mathrm{II}}]/\tau_{\mathrm{o}}c^{1/2}$ under mode II loading ($p = 0$ and $q = -\tau_{\mathrm{o}}$) for an interface crack as a function of graded interlayer thickness $h/2c$ for different values of nonhomogeneity parameter βc ($\theta = 90°$ and $d/c = 0.0$).

tends to zero. It is noted that for $\theta = 90°$, the coupling stress intensity factors as shown in Fig. 4 are equal in magnitude and opposite in sign at the other crack tip.

The variations of stress intensity factors for the arbitrarily oriented crack are next provided in Figs. 5–10 as a function of the crack orientation angle θ. With the crack surface being loaded by uniform normal traction and for $d/c = 0.0$ and $h/2c = 0.5$, Fig. 5 illustrates the results for different elastic moduli ratios E_3/E_1. In this figure, the crack is shown to experience the considerable mixed-mode deformation arising from the lack of material and geometric symmetry about the crack plane. Such a coupling effect in terms of the values of mixed-mode stress intensity factors is seen to be more obvious when θ becomes greater and, at the same time, E_3/E_1 is less than unity. Specifically, in addition to the fact that the values of K_{I} increase with decreasing E_3/E_1, those of both K_{I} and K_{II} are being enlarged with increasing θ when the crack is in the stiff constituent ($E_3/E_1 < 1.0$), indicating the higher likelihood of brittle fracture for the greater values of θ, given the same crack surface tractions. Otherwise, the opposite behavior may prevail for $E_3/E_1 > 1.0$ that also indicates the enhanced fracture resistance for the crack in a compliant constituent by the adjacent stiffer material for greater θ.

Fig. 6 shows the mixed-mode stress intensity factors induced under the uniform shear crack surface traction for different elastic moduli ratios E_3/E_1 and for $d/c = 0.0$ and $h/2c = 0.5$. Similar to the previous case of a uniformly pressurized crack, there is a substantial increase in the magnitude of major component of stress intensity factors K_{II} for $E_3/E_1 < 1.0$ and a decrease if $E_3/E_1 > 1.0$ when compared with those for homogeneous media. As seen in Fig. 6a, the stress intensity factors at the crack tip a may not undergo monotonic variations with θ, especially when the values of E_3/E_1 are much less than unity, while such a trend is not observed for the crack tip away from the interlayer as illustrated in Fig. 6b. To be mentioned now is that with the crack surface being loaded only in shear mode, depending on the values of θ and E_3/E_1, the coupling stress intensity factor K_{I} may be negative with the occurrence of partial or full crack closure. If

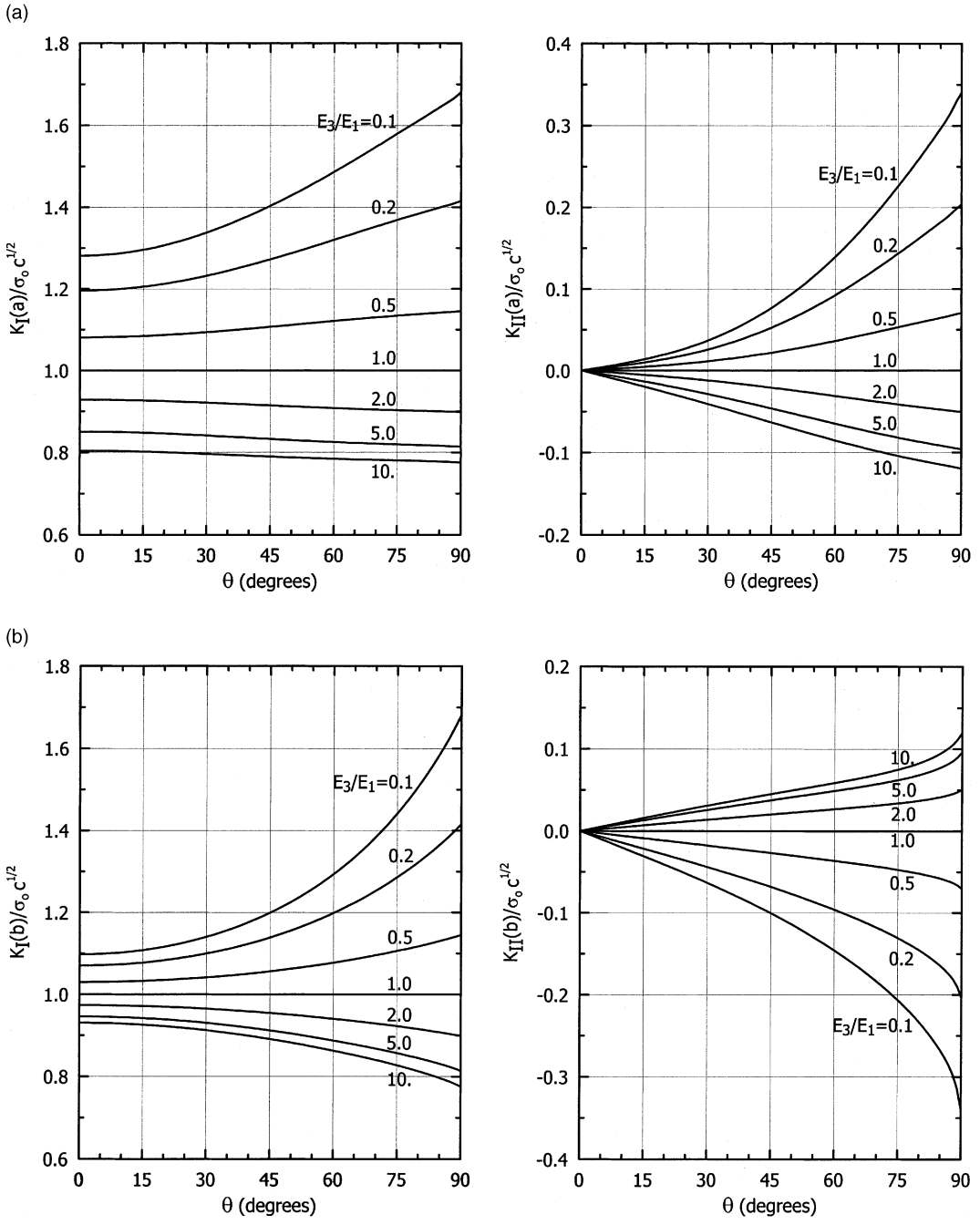

Fig. 5. Mixed-mode stress intensity factors: (a) $[K_I(a), K_{II}(a)]/\sigma_o c^{1/2}$; (b) $[K_I(b), K_{II}(b)]/\sigma_o c^{1/2}$ under mode I loading ($p = -\sigma_o$ and $q = 0$) versus crack orientation angle θ for different elastic moduli ratios E_3/E_1 ($h/2c = 0.5$ and $d/c = 0.0$).

taken separately, even though the implicit assumption of a frictionless open crack model is violated, such negative solutions can be used under the combined actions of normal and shear loadings that give rise to the positive values of superimposed K_I at both the crack tips, as will be discussed in the next section.

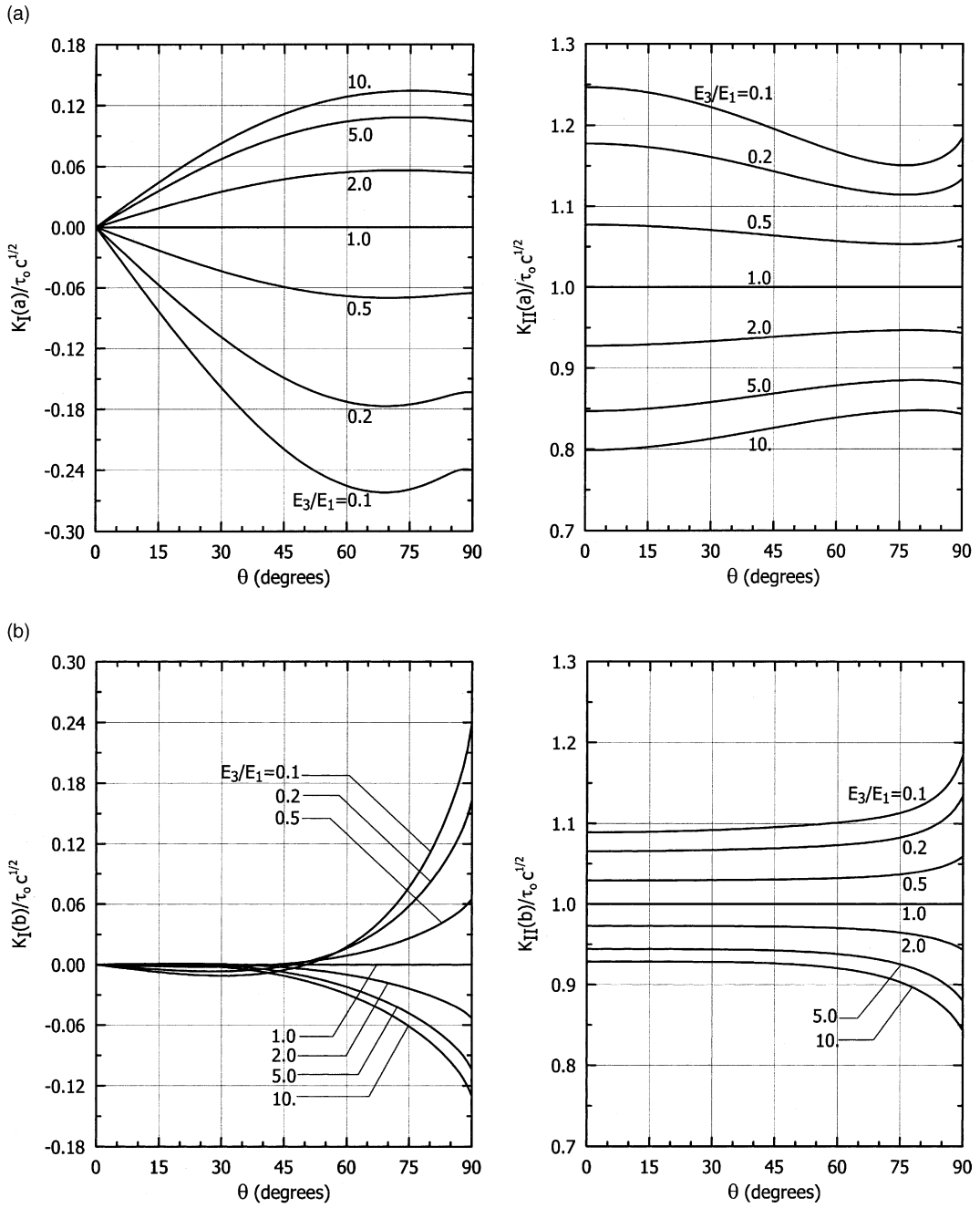

Fig. 6. Mixed-mode stress intensity factors: (a) $[K_I(a), K_{II}(a)]/\tau_o c^{1/2}$; (b) $[K_I(b), K_{II}(b)]/\tau_o c^{1/2}$ under mode II loading ($p = 0$ and $q = -\tau_o$) versus crack orientation angle θ for different elastic moduli ratios E_3/E_1 ($h/2c = 0.5$ and $d/c = 0.0$).

Figs. 7 and 8 illustrate the effect of crack distance d/c from the nominal interface when the crack is subjected to uniform normal and shear crack surface tractions, respectively, for the fixed interlayer

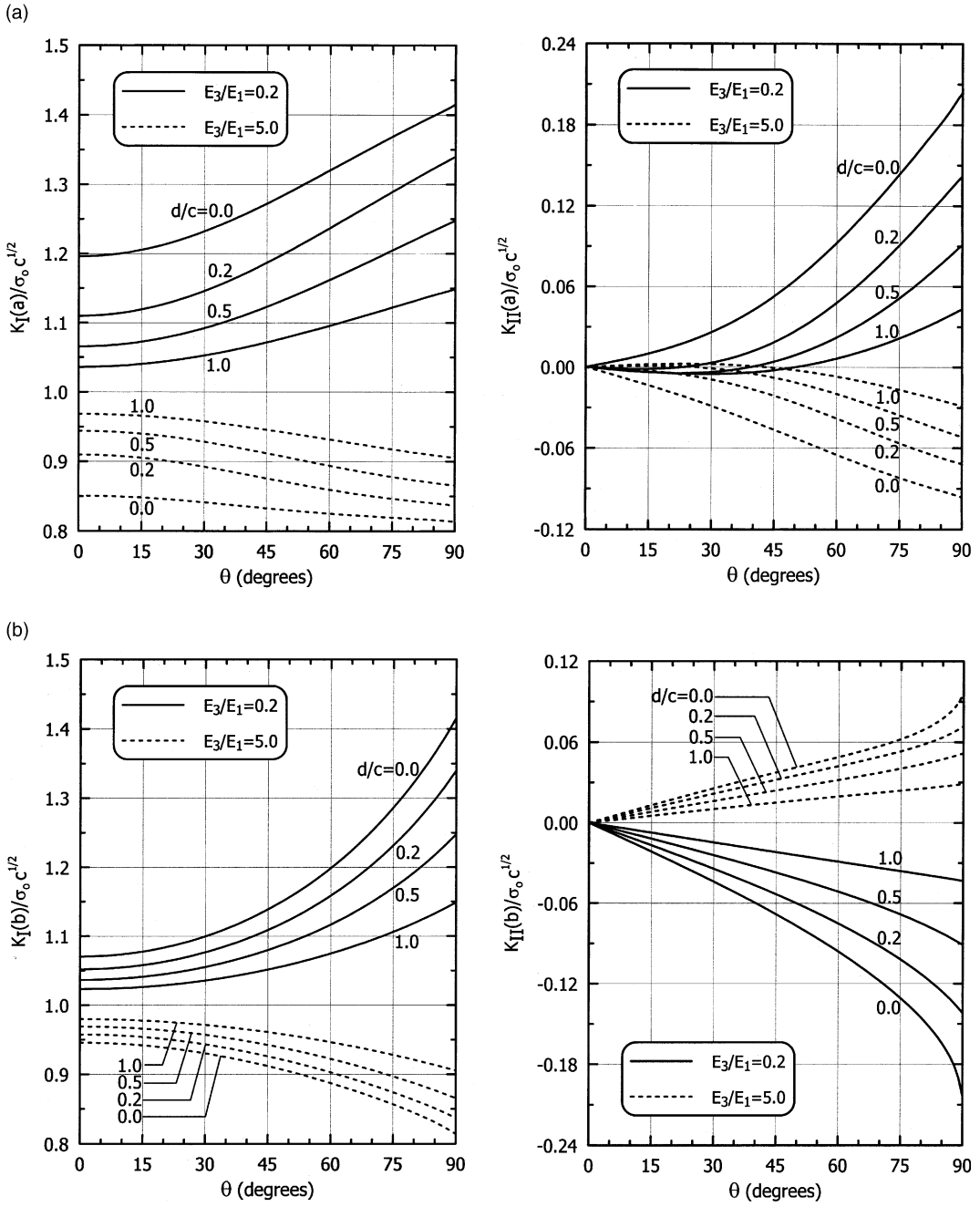

Fig. 7. Mixed-mode stress intensity factors: (a) $[K_{\mathrm{I}}(a), K_{\mathrm{II}}(a)]/\sigma_{\mathrm{o}}c^{1/2}$; (b) $[K_{\mathrm{I}}(b), K_{\mathrm{II}}(b)]/\sigma_{\mathrm{o}}c^{1/2}$ under mode I loading ($p = -\sigma_{\mathrm{o}}$ and $q = 0$) versus crack orientation angle θ for different crack locations d/c and elastic moduli ratios E_3/E_1 ($h/2c = 0.5$).

thickness, $h/2c = 0.5$. Under both the crack surface loadings, a generic trend to be seen is that the major components of stress intensity factors decrease with decreasing d/c for $E_3/E_1 = 5.0$, implying the more pronounced constraints by the stiffer constituent as the crack is closer to the interface with the interlayer,

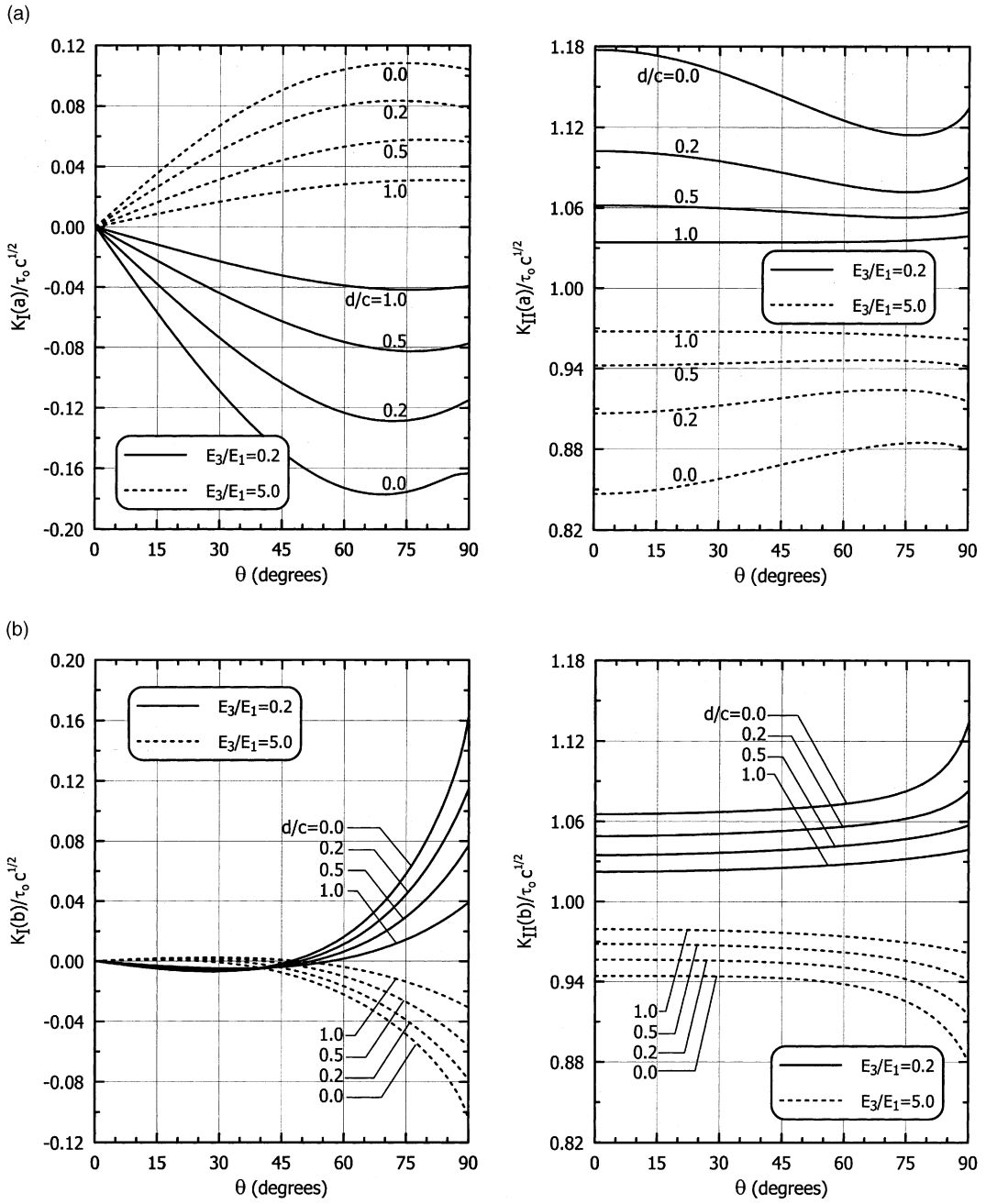

Fig. 8. Mixed-mode stress intensity factors: (a) $[K_I(a), K_{II}(a)]/\tau_o c^{1/2}$; (b) $[K_I(b), K_{II}(b)]/\tau_o c^{1/2}$ under mode II loading ($p = 0$ and $q = -\tau_o$) versus crack orientation angle θ for different crack locations d/c and elastic moduli ratios E_3/E_1 ($h/2c = 0.5$).

while the opposite behavior is encountered for $E_3/E_1 = 0.2$. When the crack is located farther away from the interface, however, the stress intensity factors become less sensitive to the variations of crack angle and material parameters and the solutions would approach those for a crack in an infinite homogeneous plane.

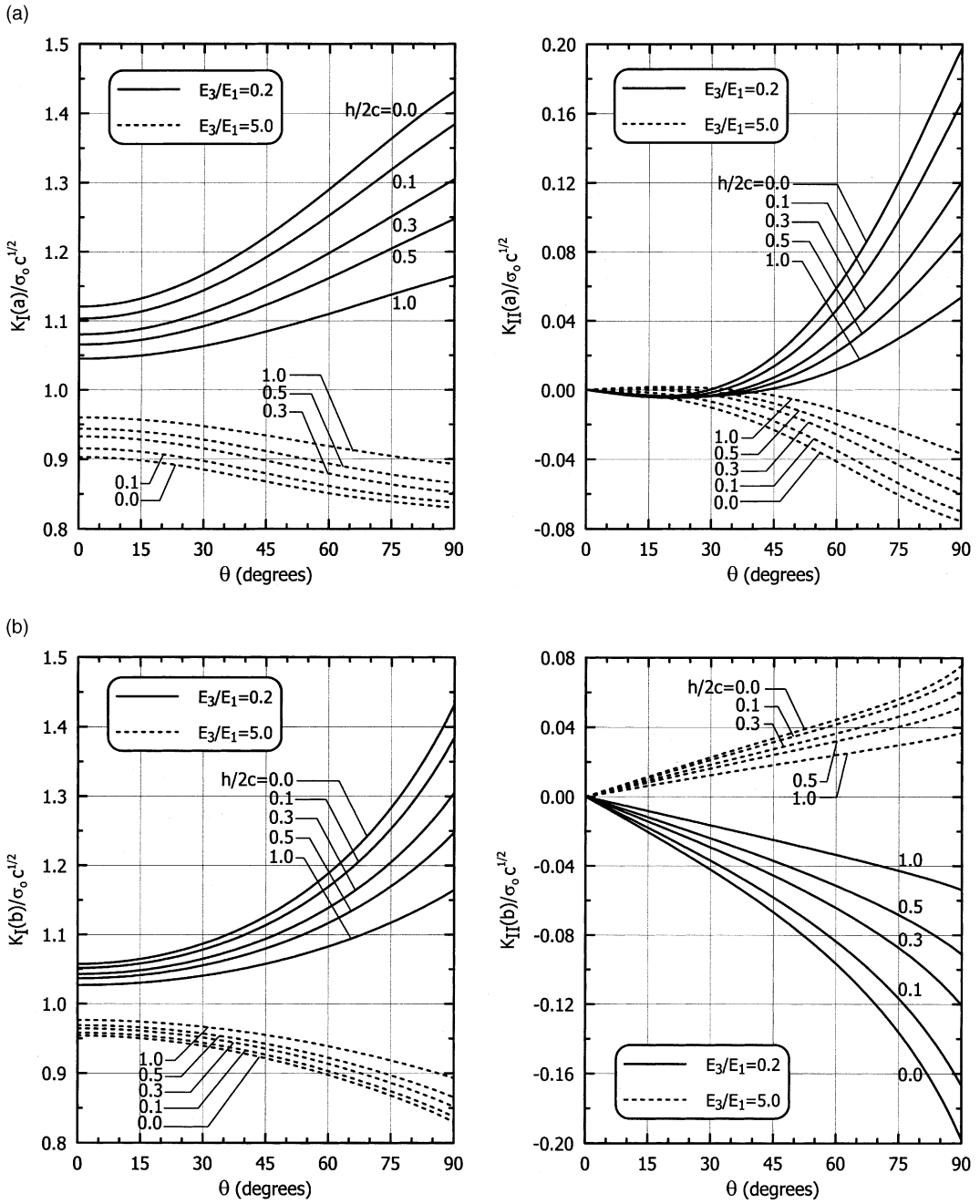

Fig. 9. Mixed-mode stress intensity factors: (a) $[K_{\mathrm{I}}(a), K_{\mathrm{II}}(a)]/\sigma_{\mathrm{o}}c^{1/2}$; (b) $[K_{\mathrm{I}}(b), K_{\mathrm{II}}(b)]/\sigma_{\mathrm{o}}c^{1/2}$ under mode I loading ($p = -\sigma_{\mathrm{o}}$ and $q = 0$) versus crack orientation angle θ for different graded interlayer thicknesses $h/2c$ and elastic moduli ratios E_3/E_1 ($d/c = 0.5$).

To be noted is that for $\theta = 90°$ and $d/c > 0.0$, the results for the subinterface crack parallel to the interface are generated.

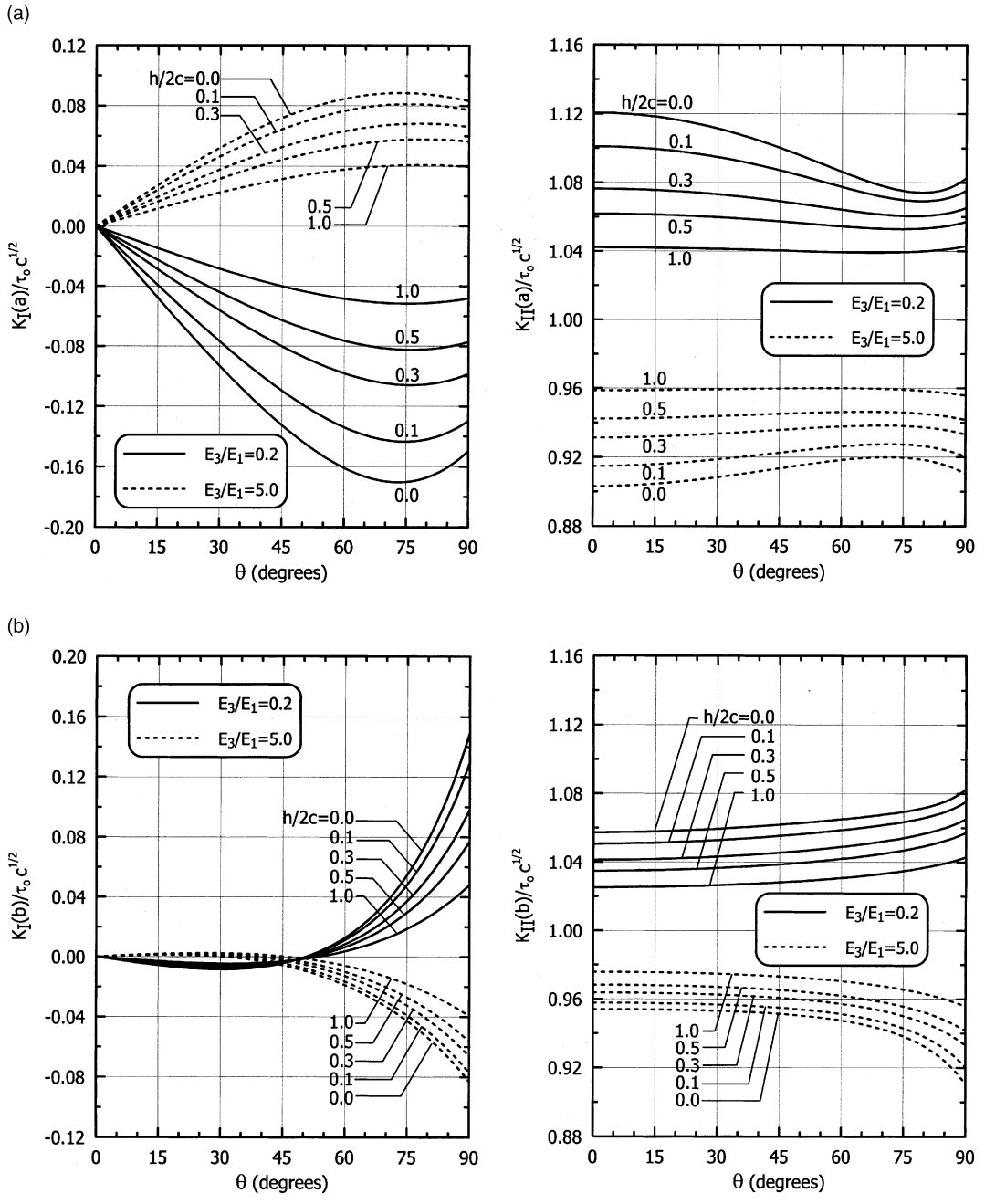

Fig. 10. Mixed-mode stress intensity factors: (a) $[K_{\mathrm{I}}(a), K_{\mathrm{II}}(a)]/\tau_{\mathrm{o}}c^{1/2}$; (b) $[K_{\mathrm{I}}(b), K_{\mathrm{II}}(b)]/\tau_{\mathrm{o}}c^{1/2}$ under mode II loading ($p = 0$ and $q = -\tau_{\mathrm{o}}$) versus crack orientation angle θ for different graded interlayer thicknesses $h/2c$ and elastic moduli ratios E_3/E_1 ($d/c = 0.5$).

With the crack tip a located at some distance from the graded interlayer as $d/c = 0.5$, the stress intensity factors for different interlayer thicknesses, $h/2c$, are plotted in Figs. 9 and 10 under the uniform normal and shear crack surface tractions, respectively. A common feature to be remarked is that an increase in $h/2c$

leads to a decrease in the magnitude of major stress intensity factors for $E_3/E_1 = 0.2$, and the reverse response is obtained for $E_3/E_1 = 5.0$. On the other hand, the magnitude of coupling stress intensity factors becomes smaller when $h/2c$ increases regardless of the material combinations, which is similar to the effect of increasing the crack distance d/c as in Figs. 7 and 8. Above trend with $h/2c$, including the limiting case of $h/2c = 0.0$, indicates that when the crack is in the stiffer constituent, the presence of a graded interlayer with the greater thickness would be more effective in shielding the crack, offsetting the influence of the adjacent compliant constituent. If the thickness ratio $h/2c$ is increased even further, the effect of θ would become, as expected, insignificant such that in conjunction with the dilution of the degree of nonhomogeneity within the interlayer, the solutions would also tend to those for the homogeneous counterpart.

6.2. Remote biaxial loading

The mixed-mode stress intensity factors under the biaxial loading condition are examined. As shown in Fig. 11, the external stresses, σ^{∞}_{iyy}, $i = 1, 2, 3$, and σ^{∞}_{xx}, are applied sufficiently far away from the crack region. The displacement continuity at the nominal interfaces requires that such stresses at infinity are not independent, but must be of necessity related in such a manner as to produce one of the constant strains in the y-direction at points remote from the crack. The far-field stresses should then have the following relations as

$$\sigma^{\infty}_{2yy} = \frac{\mu_2}{\mu_1}\sigma^{\infty}_{1yy} + \left(\frac{3-\kappa}{1+\kappa}\right)\left(1 - \frac{\mu_2}{\mu_1}\right)\sigma^{\infty}_{xx} \tag{46a}$$

$$\sigma^{\infty}_{3yy} = \frac{\mu_3}{\mu_1}\sigma^{\infty}_{1yy} + \left(\frac{3-\kappa}{1+\kappa}\right)\left(1 - \frac{\mu_3}{\mu_1}\right)\sigma^{\infty}_{xx} \tag{46b}$$

where $\mu_2 = E_o\, e^{\beta}_x/2(1+\nu) \rightarrow \mu_i = E_i/2(1+\nu)$

Via the superposition principle, the above problem of a traction-free crack can be considered as that of a crack loaded by the statically self-equilibrating tractions which are needed for investigating the local crack-tip behavior in terms of the stress intensity factors. As a result, under the prescribed biaxial loading condition, the equivalent crack surface tractions in Eq. (6b) are obtained for the crack angle θ as

$$p(x_1) = -\left(\sigma^{\infty}_{1yy}\cos^2\theta + \sigma^{\infty}_{xx}\sin^2\theta\right), \quad q(x_1) = -\left(\sigma^{\infty}_{1yy} - \sigma^{\infty}_{xx}\right)\cos\theta\sin\theta; \quad a < x_1 < b \tag{47}$$

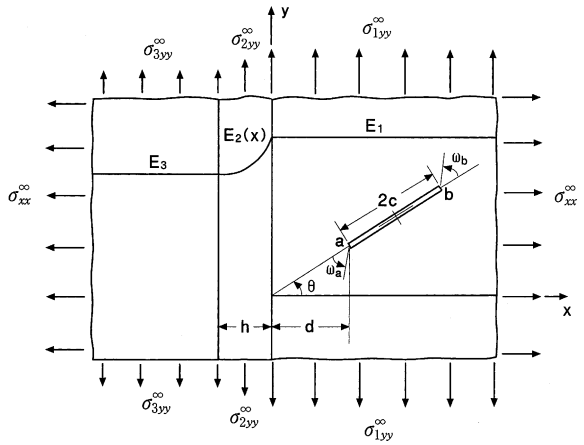

Fig. 11. Bonded half-planes with a graded interfacial zone and an inclined crack subjected to remote biaxial loading.

In order to quantify the biaxial load effects, it is assumed that $\sigma^{\infty}_{1yy} = p_o$ and $\sigma^{\infty}_{xx} = \lambda_o p_o$ where p_o is a constant and λ_o is a parameter measuring the degree of load biaxiality. In this case, the corresponding values of the stress intensity factors can be readily estimated by using those in the preceding section that are obtained under the uniform crack surface tractions. With the normalized stress intensity factors for each type of the uniform crack surface tractions expressed as

$$\left(K^o_{11}, K^o_{21}\right) = \left(\frac{K_I}{\sigma_o\sqrt{c}}, \frac{K_{II}}{\sigma_o\sqrt{c}}\right), \quad \left(K^o_{12}, K^o_{22}\right) = \left(\frac{K_I}{\tau_o\sqrt{c}}, \frac{K_{II}}{\tau_o\sqrt{c}}\right) \tag{48}$$

where the first subscript $i = 1, 2$, in K^o_{ij} denotes the tensile and shearing mode stress intensities, respectively, and the second subscript $j = 1, 2$, refers to the uniform normal $(p = -\sigma_o, q = 0)$ and shear $(p = 0, q = -\tau_o)$ tractions applied on the crack surface, respectively, and those for the remote biaxial loading can be obtained as

$$\left\{\begin{array}{c} K_I \\ K_{II} \end{array}\right\} = p_o\sqrt{c}\left(\cos^2\theta + \lambda_o \sin^2\theta\right)\left\{\begin{array}{c} K^o_{11} \\ K^o_{21} \end{array}\right\} + p_o\sqrt{c}(1-\lambda_o)\cos\theta\sin\theta\left\{\begin{array}{c} K^o_{12} \\ K^o_{22} \end{array}\right\} \tag{49}$$

Fig. 12 shows the variations of mixed-mode stress intensity factors obtained for the homogeneous material that coincide exactly with the closed form solution given by Sih et al. (1962). For the two material combinations $E_3/E_1 = 0.2$ and $E_3/E_1 = 5.0$, the values of the stress intensity factors are plotted in Figs. 13 and 14, respectively, with the crack location and the interlayer thickness specified as $d/c = 0.0$ and $h/2c = 0.5$. Under the combined action of normal and shear tractions, the crack closure does not occur provided $\lambda_o > 0$ as can be depicted from Figs. 13a and 14a. Of particular interest for this trimaterial system with a graded interlayer is that as shown in Figs. 13b and 14b, the values of K_{II} may change sign depending on the crack orientation angle θ and the degree of load biaxiality λ_o. The physical consequence of this sign change may be the crack growth from its tips in the directions other than that of the original crack.

To predict the onset and direction of incipient kinking of the original unextended crack, an assumption of the local homogeneity and isotropy of the medium is invoked with respect to its fracture resistance, especially in a small region close to the crack tip that may intersect the nominal interface with the graded

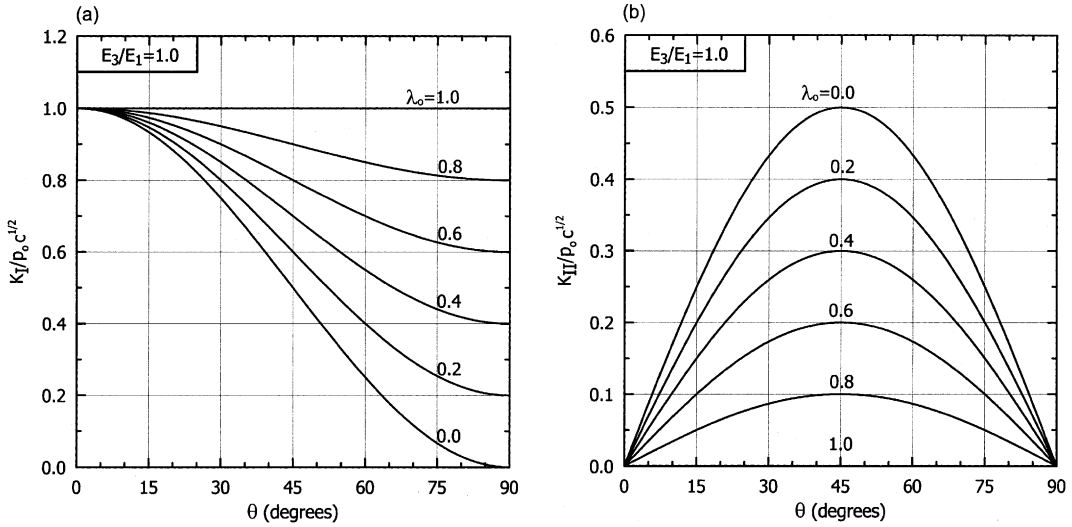

Fig. 12. Mixed-mode stress intensity factors: (a) $K_I/p_o c^{1/2}$; (b) $K_{II}/p_o c^{1/2}$ under biaxial loading versus crack orientation angle θ in the homogeneous medium $(E_3/E_1 = 1.0)$.

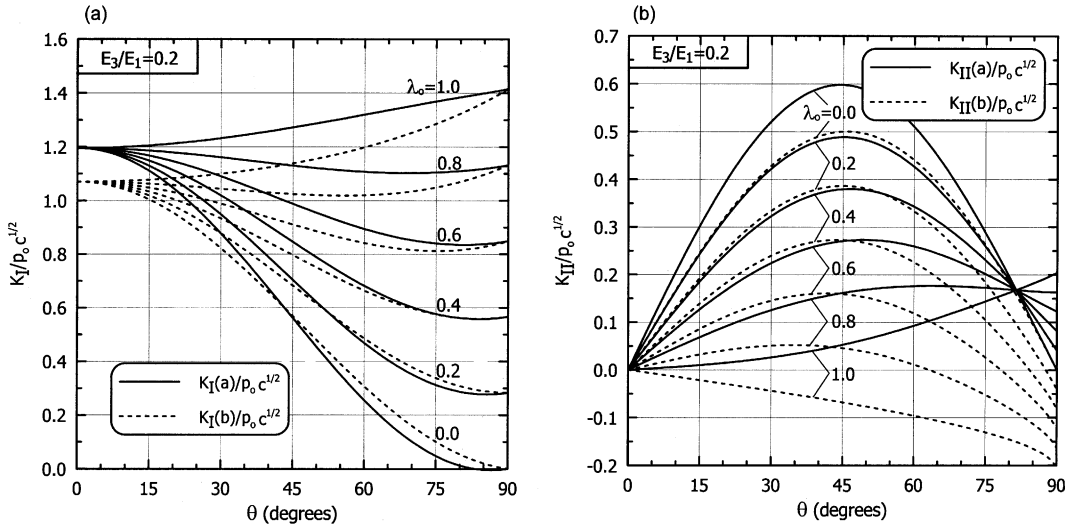

Fig. 13. Mixed-mode stress intensity factors: (a) $K_I/p_o c^{1/2}$; (b) $K_{II}/p_o c^{1/2}$ under biaxial loading versus crack orientation angle θ in the bonded media with a graded interlayer ($E_3/E_1 = 0.2$, $h/2c = 0.5$, and $d/c = 0.0$).

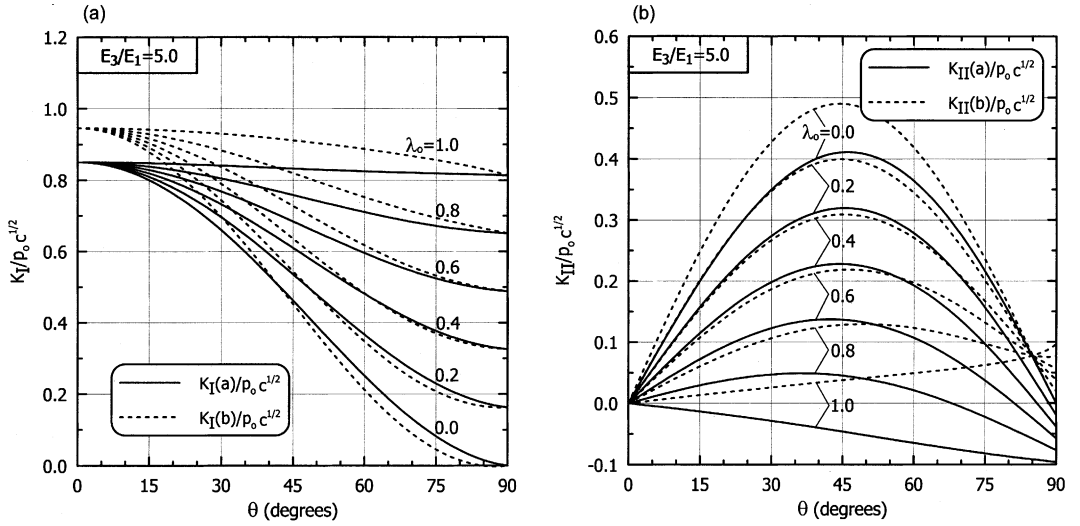

Fig. 14. Mixed-mode stress intensity factors: (a) $K_I/p_o c^{1/2}$; (b) $K_{II}/p_o c^{1/2}$ under biaxial loading versus crack orientation angle θ in the bonded media with a graded interlayer ($E_3/E_1 = 5.0$, $h/2c = 0.5$, and $d/c = 0.0$).

interlayer. The maximum principal stress criterion is thus applied such that the crack would tend to grow along the radial planes at angles ω_i, $i = a, b$, determined by the root of the quadratic equation given as (Erdogan and Sih, 1963)

$$\tan^2\frac{\omega_i}{2} - \frac{1}{2}\frac{K_I}{K_{II}}\tan\frac{\omega_i}{2} - \frac{1}{2} = 0; \quad i = a, b \tag{50}$$

where the particular choice of the root is dictated by the following condition

$$\left(K_{\mathrm{I}}\cos\frac{\omega_i}{2}-3K_{\mathrm{II}}\sin\frac{\omega_i}{2}\right)>0;\quad i=a,b \tag{51}$$

and ω_i, $i=a,b$, are measured counterclockwise at the crack tips from the original crack plane. With such cleavage angles calculated, the effective tensile mode stress intensity factor K_{e} can be defined as a useful estimate of the tendency for crack growth as (Broek, 1986)

$$K_{\mathrm{e}}=\cos^2\frac{\omega_i}{2}\left(K_{\mathrm{I}}\cos\frac{\omega_i}{2}-3K_{\mathrm{II}}\sin\frac{\omega_i}{2}\right) \tag{52}$$

in which the crack growth is then assumed to initiate in the directions of ω_i, $i=a,b$, when $K_{\mathrm{e}}>K_{\mathrm{IC}}$, the local plane strain fracture toughness of the material, and the kink is formed at the crack tips.

Subsequently, Figs. 15–17 illustrate the effects of crack angle θ and biaxial parameter λ_{o} on the probable cleavage directions and the corresponding values of effective tensile mode stress intensity factor K_{e}. To be observed from Fig. 15a is that for the inclined crack in the homogeneous plane, the cleavage angles are all negative for $0\leqslant\lambda_{\mathrm{o}}<1$, i.e., in a clockwise direction and the deviation from the main crack plane decreases as the load becomes more biaxial. When $\theta=90^\circ$ and $\lambda_{\mathrm{o}}>0$, however, the crack is subjected to pure mode I loading and the crack grows along its original direction. When the crack is in the stiffer constituent as $E_3/E_1=0.2$, with the crack location and the interlayer thickness being the same as in Figs. 13, 14, and 16a reveals that in the biaxially loaded state, the crack growth at the tip b may occur in a counterclockwise direction as $\omega_b>0$ depending on the angle θ and the load biaxiality λ_{o}, making a noteworthy contrast to the homogeneous counterpart. On the other hand, the cleavage angle ω_a is all negative. For the crack in a less stiff material as $E_3/E_1=5.0$, the reverse behavior exists as shown in Fig. 16b such that ω_a may have different sign, while ω_b is all negative. Hence, for relatively large values of θ and λ_{o}, it is probable that the crack growth would be toward or away from the graded interlayer to be in the direction of decreasing stiffness of the bonded media. Another notable feature apparent in Fig. 17 is that similar to the results in Fig. 15b, the magnitude and variations of effective tensile mode stress intensities K_{e} with θ are quite

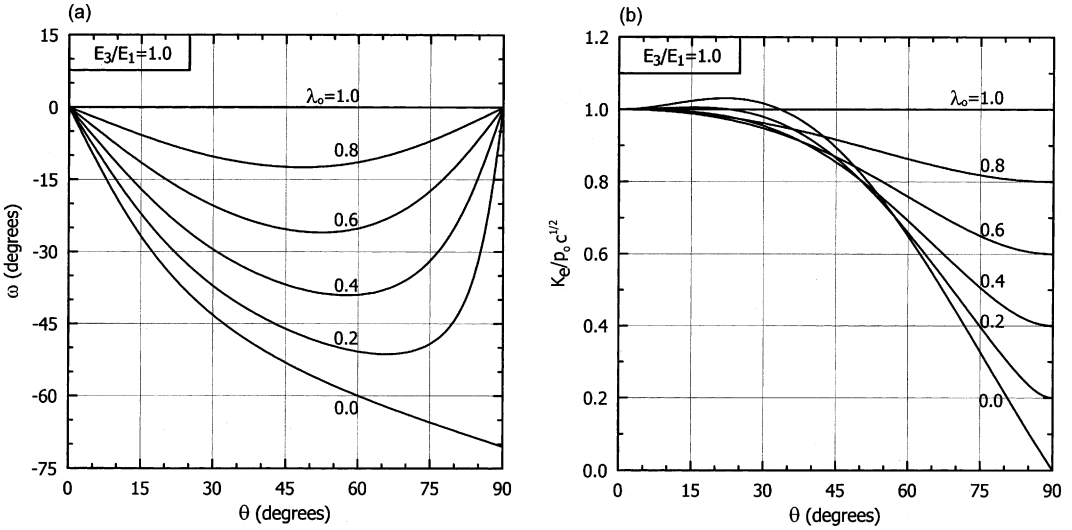

Fig. 15. Variations of: (a) cleavage angles ω; (b) effective tensile mode stress intensity factors $K_{\mathrm{e}}/p_{\mathrm{o}}c^{1/2}$ as a function of crack orientation angle θ in the homogeneous medium under biaxial loading ($E_3/E_1=1.0$).

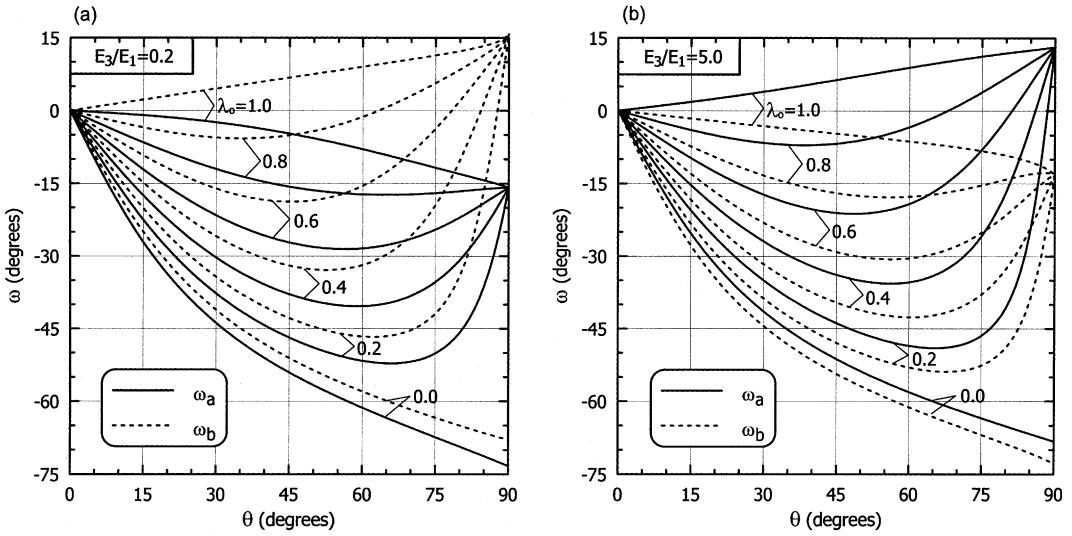

Fig. 16. Variations of cleavage angles ω for: (a) $E_3/E_1 = 0.2$; (b) $E_3/E_1 = 5.0$ as a function of crack orientation angle θ in the bonded media with a graded interlayer under biaxial loading ($h/2c = 0.5$ and $d/c = 0.0$).

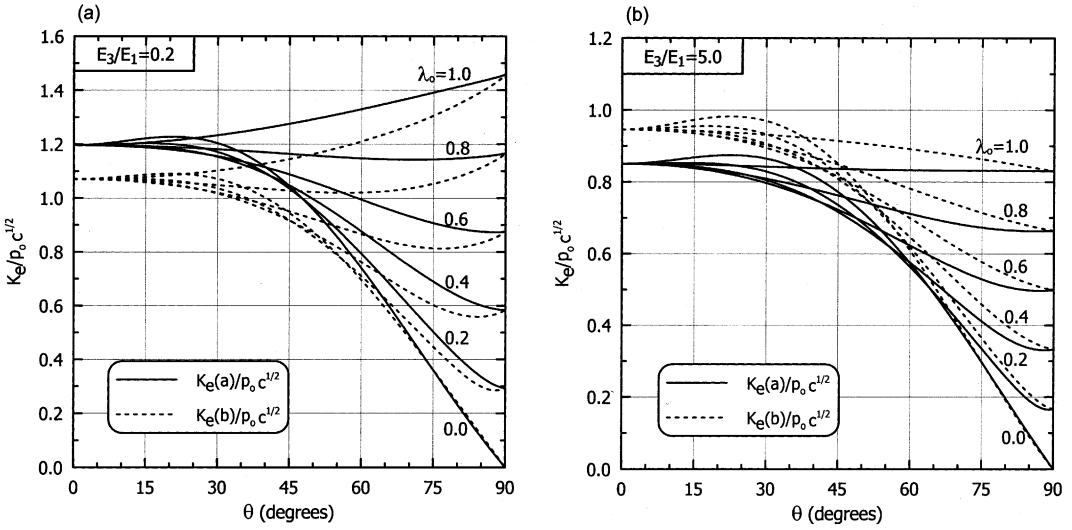

Fig. 17. Variations of effective tensile mode stress intensity factors $K_c/p_0c^{1/2}$ for: (a) $E_3/E_1 = 0.2$; (b) $E_3/E_1 = 5.0$ as a function of crack orientation angle θ in the bonded media with a graded interlayer under biaxial loading ($h/2c = 0.5$ and $d/c = 0.0$).

comparable to the mode I stress intensity factors for the main crack. This may be indicative of a fact that while the direction of probable crack cleavage is mainly controlled by the magnitude and sign of K_{II} the propensity for the crack growth is dominated by the values of K_I.

Based on the idea that the thickness as well as the properties of the interfacial zone may affect the direction of crack growth, the cleavage angles are provided in Fig. 18 as a function of interlayer thickness $h/2c$ under uniaxial loading ($\lambda_o = 0$). For the given crack orientation θ and $d/c = 0.0$, it is shown that the

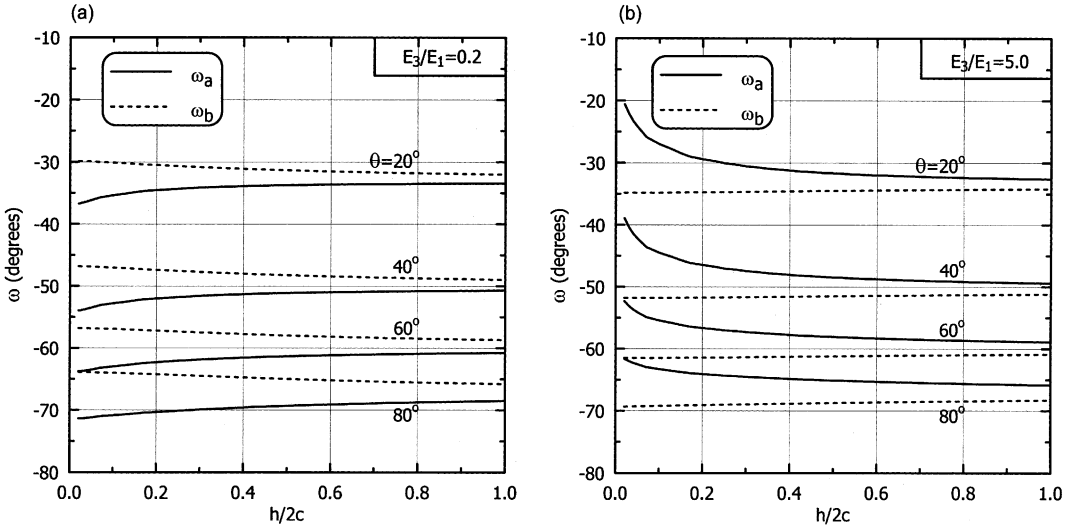

Fig. 18. Variations of cleavage angles ω for: (a) $E_3/E_1 = 0.2$; (b) $E_3/E_1 = 5.0$ as a function of graded interlayer thickness $h/2c$ for different values of crack orientation angle θ in the bonded media under uniaxial loading ($d/c = 0.0$ and $\lambda_o = 0.0$).

cleavage angles are approaching those in the homogeneous medium as $h/2c$ increases, although the values of ω_a are seen to be more sensitive to the variation of interlayer thickness.

7. Closing remarks

The problem of an inclined crack in bonded media with a graded nonhomogeneous interlayer has been investigated by deriving a corresponding system of singular integral equations, based on the use of basic plane elasticity equations and the Fourier integral transform technique. Parametric studies were conducted so that the mixed-mode stress intensity factors were evaluated, demonstrating several unique and salient features concerning the local behavior of an arbitrarily oriented crack strongly affected by the material and geometric configurations of the bonded media in conjunction with the elastic property gradation within the interlayer. In an effort to further quantify the crack-tip behavior, the probable cleavage angles of the original crack were estimated under the biaxially loaded condition, together with the values of effective tensile mode stress intensity factors. In applications of the results obtained in this study, it is likely that the inclined crack nearby or touching the graded interlayer could be arrested by or advances into the adjacent materials, depending upon the relative magnitude of toughnesses of the constituents. Additional possibilities of practical interest that may arise are that the crack may tend to grow and then reflect back at some angle or debonding initiates along the lines of nominal interfaces to interact and coalesce with the original growing crack. It is anticipated that the versatility of the current analytical solution procedure could be extended to resolve such more involved issues.

References

Ashbaugh, N., 1975. Stress solution for a crack at an arbitrary angle to an interface. Int. J. Fract. 11, 205–219.
Atkinson, C., 1977. On stress singularities and interfaces in linear elastic fracture mechanics. Int. J. Fract. 13, 807–820.

Babaei, R., Lukasiewicz, S.A., 1998. Dynamic response of a crack in a functionally graded material between two dissimilar half-planes under anti-plane shear impact load. Engng. Fract. Mech. 60, 479–487.
Bao, G., Cai, H., 1997. Delamination cracking in functionally graded coating/metal substrate systems. Acta Materialia 45, 1055–1066.
Beghini, M., Bertini, L., Fontanari, V., 1999. Stress intensity factors for an inclined edge crack in a semiplane. Engng. Fract. Mech. 62, 607–613.
Bogy, D.B., 1971. On the plane elastostatic problem of a loaded crack terminating at a material interface. ASME J. Appl. Mech. 38, 911–918.
Broek, D., 1986. Elementary Engineering Fracture Mechanics, fourth ed. Kluwer Academic, The Netherlands.
Chen, Y.F., 1990. Interface crack in nonhomogeneous bonded materials of finite thickness. Ph.D. Dissertation, Lehigh University.
Choi, H.J., 1996a. An analysis of cracking in a layered medium with a functionally graded nonhomogeneous interface. ASME J. Appl. Mech. 63, 479–486.
Choi, H.J., 1996b. Bonded dissimilar strips with a crack perpendicular to the functionally graded interface. Int. J. Solids Struct. 33, 4101–4117.
Choi, H.J., 1997. A periodic array of cracks in a functionally graded nonhomogeneous medium loaded under in-plane normal and shear. Int. J. Fract. 88, 107–128.
Choi, H.J., Lee, K.Y., Jin, T.E., 1998a. Collinear cracks in a layered half-plane with a graded nonhomogeneous interfacial zone – part I: mechanical response. Int. J. Fract. 94, 103–122.
Choi, H.J., Jin, T.E., Lee, K.Y., 1998b. Collinear cracks in a layered half-plane with a graded nonhomogeneous interfacial zone – part II: thermal shock response. Int. J. Fract. 94, 123–135.
Davis, P.J., Rabinowitz, P., 1984. Method of Numerical Integration, second ed. Academic Press, Florida.
Delale, F., Bakirtas, I., Erdogan, F., 1979. The problem of an inclined crack in an orthotropic strip. ASME J. Appl. Mech. 46, 90–96.
Delale, F., Erdogan, F., 1988. On the mechanical modeling of the interfacial region in bonded half-planes. ASME J. Appl. Mech. 55, 317–324.
Eischen, J.W., 1987. Fracture of nonhomogeneous materials. Int. J. Fract. 34, 3–22.
Erdogan, F., 1978. Mixed boundary value problems in mechanics. Mech. Today 4, 1–86.
Erdogan, F., Aksogan, O., 1974. Bonded half planes containing an arbitrarily oriented crack. Int. J. Solids Struct. 10, 569–585.
Erdogan, F., Arin, K., 1975. A half plane and a strip with an arbitrarily located crack. Int. J. Fract. 11, 191–204.
Erdogan, F., Kaya, A.C., Joseph, P.F., 1991. The crack problem in bonded nonhomogeneous materials. ASME J. Appl. Mech. 58, 410–418.
Erdogan, F., Sih, G.C., 1963. On the crack extension in plates under plane loading and transverse shear. ASME J. Basic Engng. 85, 519–527.
Gradshteyn, I.S., Ryzhik, I.M., 1980. Table of Integrals, Series, and Products. Academic Press, New York.
Gu, P., Asaro, R.J., 1997. Crack deflection in functionally graded materials. Int. J. Solids Struct. 34, 3085–3098.
Isida, M., Noguchi, H., 1993. Arbitrary array of cracks in bonded half planes subjected to various loadings. Engng. Fract. Mech. 46, 365–380.
Jin, Z.-H., Batra, R.C., 1996. Interface cracking between functionally graded coatings and a substrate under antiplane shear. Int. J. Engng. Sci. 34, 1705–1716.
Jin, Z.-H., Noda, N., 1994. Crack-tip singular fields in nonhomogeneous materials. ASME J. Appl. Mech. 61, 738–740.
Kim, H.K., Lee, S.B., 1996. Stress intensity factors of an oblique edge crack subjected to normal and shear tractions. Theoret. Appl. Fract. Mech. 25, 147–154.
Koizumi, M., 1993. The concept of FGM. In: Holt, J.B., et al. (Eds.), Ceramic Transactions vol. 34. Functionally Gradient Materials. American Ceramic Society. Ohio, pp. 3–10.
Krenk, S., 1975. On the elastic strip with an internal crack. Int. J. Solids Struct. 11, 693–708.
Lee, Y.-D., Erdogan, F., 1994. Residual/thermal stresses in FGM and laminated thermal barrier coatings. Int. J. Fract. 69, 145–165.
Martin, P.A., 1992. Tip behaviour for cracks in bonded inhomogeneous materials. J. Engng. Math. 26, 467–480.
Muskhelishvili, N.I., 1953. Singular Integral Equations. Noordhoff, Groningen, The Netherlands.
Ozturk, M., Erdogan, F., 1996. Axisymmetric crack problem in bonded materials with a graded interfacial region. Int. J. Solids Struct. 33, 193–219.
Parameswaran, V., Shukla, A., 1999. Crack-tip stress fields for dynamic fracture in functionally gradient materials. Mech. Mater. 31, 579–596.
Rayaprolu, D.B., Rooke, D.P., 1998. Influence functions for inclined edge cracks. Fatigue Fract. Engng. Mater. 21, 761–769.
Rice, J.R., 1988. Elastic fracture mechanics concepts for interfacial cracks. ASME J. Appl. Mech. 55, 98–103.
Romeo, A., Ballarini, R., 1995. A crack very close to a bimaterial interface. ASME J. Appl. Mech. 62, 614–619.
Schovanec, L., Walton, J.R., 1988. On the order of the stress singularity for an antiplane shear crack at the interface of two bonded inhomogeneous elastic materials. ASME J. Appl. Mech. 55, 234–236.
Shbeeb, N.I., Binienda, W.K., 1999. Analysis of an interface crack for a functionally graded strip sandwiched between two homogeneous layers of finite thickness. Engng. Fract. Mech. 64, 693–720.

Sih, G.C., Paris, P.C., Erdogan, F., 1962. Crack-tip stress intensity factors for plane extension and plate bending problems. ASME J. Appl. Mech. 29, 306–312.

Suresh, S., Mortensen, A., 1997. Functionally graded metals and metal–ceramic composites: part 2 thermomechanical behaviour. Int. Mater. Rev. 42, 85–116.

Wang, X.D., Meguid, S.A., 1996. On the general treatment of an oblique crack near a bimaterial interface under antiplane loading. Int. J. Solids Struct. 33, 2485–2500.